Material Temperature Effects on Final Product Size for New Profile Ring Mill Forming Technology

by

Andrew D. McCraith

B.S. Mechanical Engineering
Massachusetts Institute of Technology, 1998

SUBMITTED TO THE DEPARTMENT OF MECHANICAL ENGINEERING IN PARTIAL FULFILLMENT OF THE REQUIREMENTS FOR THE DEGREE OF

MASTER OF SCIENCE IN MECHANICAL ENGINEERING
AT THE
MASSACHUSETTS INSTITUTE OF TECHNOLOGY

JUNE 1999

Signature of Author: _____
Department of Mechanical Engineering
May 26, 1999

Certified By: _____
Jung-Hoon Chun
Associate Professor of Mechanical Engineering
Thesis Supervisor

Accepted By: _____
Ain A. Sonin
Professor of Mechanical Engineering
Chairman, Committee for Graduate Students

Temperature Effects on the Final Product Size for the New Profile Ring Mill (PRM) Forming Technology

by

Andrew D. McCraith

Submitted to the Department of Mechanical Engineering
on May 21, 1999 in partial fulfillment of the requirements
for the degree of Master of Science in Mechanical Engineering

ABSTRACT

The new Profile Ring Mill (PRM) technology was developed to manufacture the initial preforms required for producing components of bearing assemblies. This continuous hot, single-step forming process was desired to replace the previous machining alternatives because of the increased throughput rate. The PRM technology was first incorporated into production in early 1998 at the new Tryon Peak facility. While there are several parameters that contribute to the successful operation of the PRM, like many other "hot" processes, the forming temperature is one of the most critical factors.

It was initially assumed that the entire product formed from each shell was uniform. After preliminary testing revealed that there was significant dimensional variation along the length of the shell (DVAL), the Entry Temperature Profile (ETP) model was developed to explain this phenomenon. The ETP model predicts that there is a significant variation in the shell temperature as a result of radiant cooling during the forming process. Since the forming temperature directly affects many of the factors that determine the final product size: shrinkage, elastic recovery, and equipment swelling, a change in the forming temperature results in non-uniformity in the final product size. The results of continuously measuring the shell entry temperature and the PRM main drive current over the entire forming process confirmed that variation in the forming temperature is a root cause of the DVAL. The existence of significant DVAL will continue to result in increased scrap until an in-line temperature control system has been successfully implemented.

Thesis Supervisor: Jung-Hoon Chun
Title: Associate Professor of Mechanical Engineering

ACKNOWLEDGEMENTS

There are many people who have helped make it possible for me to reach this success. Most importantly to this process have been my parents, Deane and Douglas, and my sister, Sheila. Also, I offer a special thank you to all of my friends, who continually gave me their support and advice.

I would also like to thank The Timken Company for providing me with a rewarding internship through the Engineering Internship Program. While there are many people who made this a rewarding experience, there are a few people that I must acknowledge specifically. Rosendo Fuquen, the Timken Company Program Supervisor, guided me to a suitable project and ensured a successful learning experience. The entire Profile Ring Team, especially my mentor Jim Laverick, continually provided me with constructive feedback and helped me to gather and analyze the data that I needed. Also, a special thank you to my fellow intern, David Schiller, for offering his time during numerous brain storming sessions.

Finally, I wish to thank my thesis advisor, Prof. Jung-Hoon Chun, who saved me a lot of time and wasted effort by helping me to stay focused and continually reminding me of my ultimate objective.

TABLE OF CONTENTS

List of Figures and Tables

Chapter 1: Introduction

The new Profile Ring Mill (PRM) technology was developed in order to increase the rate of production of the initial preforms required to manufacture components for bearing assemblies. An added benefit is the capability of forming individual preforms directly from a shell that has only been pierced once, but is not finished. The PRM is capable of producing profiled rings with a "straight" (constant) inside diameter (ID) of 1.0" to 2.0" and a "profiled" (non-constant) outside diameter (OD) of 2.5" to 4.5", as shown in Figure 1.1. Two mills have been installed incorporating this technology. The Tryon Peak forming mill began production in early 1998, and a similar lab stand at the Research facility began operation in mid-December of 1998.

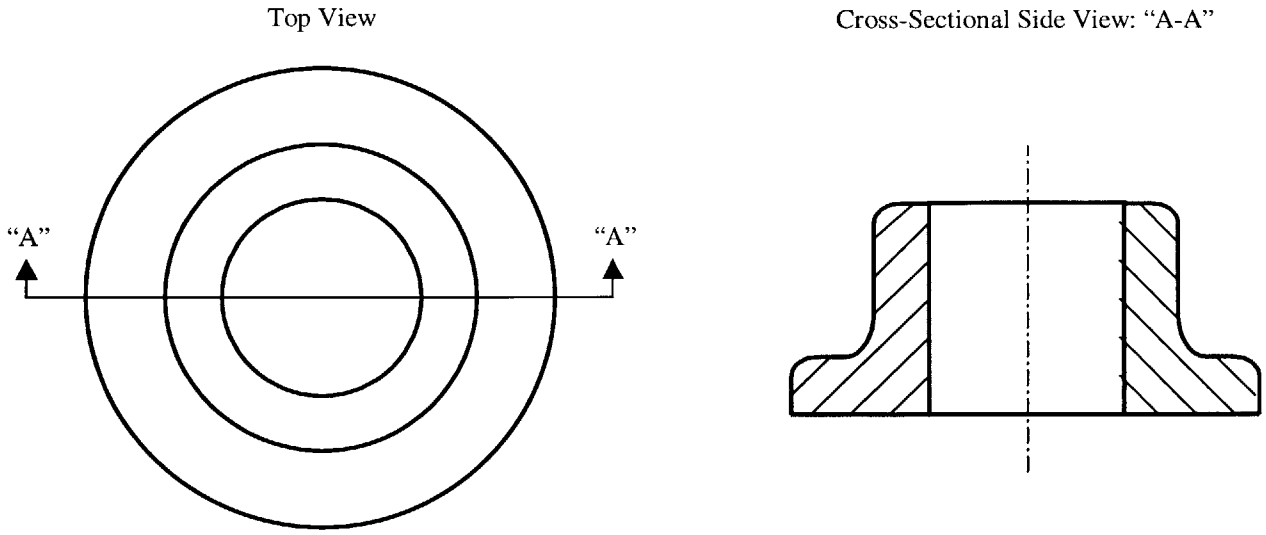

Figure 1.1. *Schematic top and side cross-sectional views of a preform.*

A preform is considered acceptable if it meets both dimensional and surface condition specifications. The dimensions need to be within both acceptable size and total-indicated run out (TIR) tolerances. Since material will be removed from the surface during subsequent finishing processes, there are tolerances for the depth of surface defects, such as laps or lack of material.

While the tolerances vary for different parts, on average the diameter's tolerance is ±0.5 mm, while the diameter's out of round tolerance and defect depth tolerances are +0.5 mm. Additional concerns about tool life, subsequent machining operations, and material handling are also important considerations in the overall product quality and productivity. While there are continuing efforts to develop a complete understanding of all the factors affecting the machine's capability to produce the most desirable product, several crucial factors have already been identified. Some of the parameters are relatively easy to control: mill speed, tooling position, tooling alignment, and the material grade. Most of the other factors are either difficult to control and to change, or their effects are not well understood: forming temperatures, mill calibration, tooling designs, and required pierced shell dimensions. Initially, the relationships between several of these key factors were investigated at the Tryon Peak facility by conducting multiple design of experiments (DOE).

The initial DOEs provided a lot of information about calibration, machine settings, and actual operation situations, but they also identified for the first time an unexpected problem of dimensional variance along the shell length (DVAL). For every shell formed, the last preforms from each shell were larger in diameter than the first preforms produced by almost 0.5 mm, or 50% of the tolerance. Since this type of defect was unexpected, there was not a known solution to remedy the problem. As with many other "hot" processes, the forming temperature is known to be a crucial factor, and was therefore quickly identified as a possible root cause.

While the forming temperature was suspected of causing the DVAL, a direct correlation to explain the phenomenon was not yet established. After analyzing the PRM equipment and process, it was possible to develop a theoretical model that related a change in the final preform size to a change in the actual forming temperature. The proposed Entry Temperature Profile (ETP) model suggests that the forming temperature decreases during each cycle because of rapid

radiant cooling. This decrease in temperature would cause the gorge to swell, increase elastic recovery, and decrease shrinkage. All three of these factors would result in an increase in the product size. Once the model was developed, it was necessary to gather experimental data to verify it.

The first series of data collected focused on the PRM equipment. Since it is difficult to monitor the roll force and the size of the forming zone directly and continuously, it was necessary to expand the ETP model to predict the PRM main drive current profile, which can be directly related to these factors. Once it was established that the roll force was increasing during the forming cycle, the next objective was to determine the forming temperature profile. Since the machine design does not allow for the actual forming temperatures to be determined, a profile of the forming temperatures during each cycle can only be approximated. Although the Shell Temperature Profile (STP) model already existed, and had been proven accurate, the STP model predicted a gradient that contradicts the profile proposed by the ETP model. The actual entry temperature profile was determined by revising the temperature monitoring system at Tryon Peak to monitor continuously the shell temperature as the shell entered the PRM.

The analysis of the experimental data verified that the forming temperature decreased during the forming process and ultimately resulted in DVAL. Once the forming temperature was determined to be the root cause of the DVAL, various process changes, equipment changes, or combinations of the two, were evaluated to address the identified cause. For each corrective action there are advantages, such as ease of installation and effectiveness, but also disadvantages, such as cost. While an ideal system of in-line heating components may be costly, an effective system of insulated enclosures and fans can be immediately implemented at minimal cost to significantly reduce the forming temperature variation, and ultimately reduce the DVAL.

Chapter 2: Background on Profile Ring Mill (PRM)

2.1. Standard Operating Procedure at Tryon Peak Production Facility

There is a five-stage process for producing preforms at the Tryon Peak production facility, as shown in Figure 2.1. All of the equipment was custom built to meet the specific needs of the Tryon Peak facility. Initially, billets are loaded manually onto a loading platform, and then automatically delivered into the desired induction furnace. If the billet temperature at the exit of the induction furnace is acceptable, the billet is transferred automatically to the piercing mill, but if the temperature is unsatisfactory, the billet is rejected into a storage bin. (The billet may be reused after cooling to room temperature, but the effects of using recycled billets have not yet been studied in depth.) After the billet is pierced to form a shell (or tube), salt is injected into the inside of the shell automatically and the shell is transferred to the Profile Ring Mill to be formed. If the shell is not going to be formed, it is transferred to a cooling bed. After the shell is formed into separate preforms, the preforms are transferred automatically to a cooling conveyor. At the exit of the cooling conveyor, the preforms are collected and transported to the finishing area.

Currently, it is not possible to accurately track the preforms through the cooling conveyor. Therefore, sample preforms are gathered during the transfer from the forming mill to the cooling conveyor and measured at the gauging station near the forming mill exit. There are two types of samples gathered: quenched and air-cooled. Frequently, one preform is manually collected from the middle of the shell, and quenched in water immediately. Although this accelerates the cooling rate and allows for more immediate gauging, this extremely rapid cooling process causes the quenched preforms to have different dimensions than a preform that underwent standard conveyor cooling. Therefore, at a less frequent rate, preforms are manually

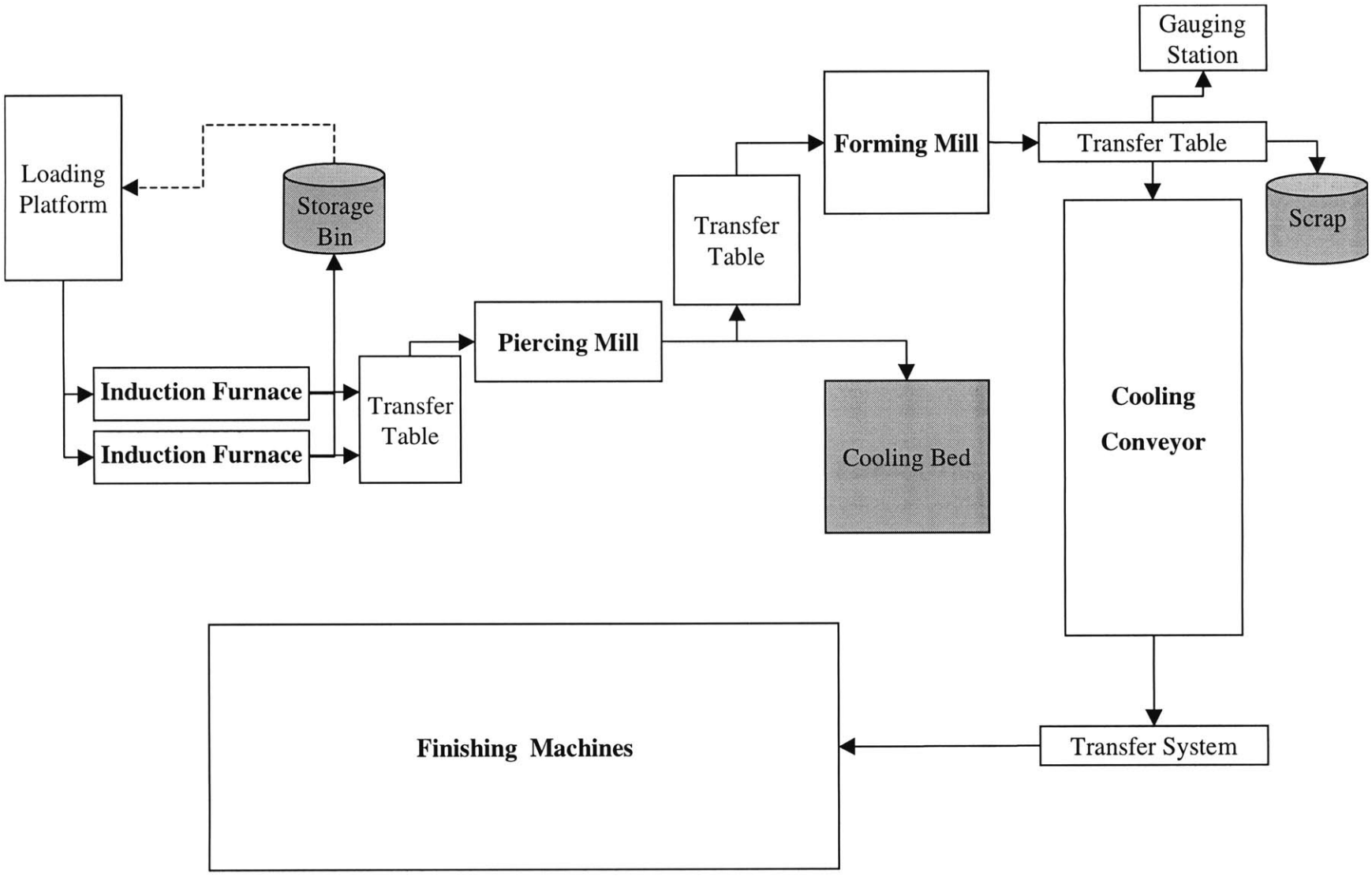

Figure 2.1. *Schematic of Tryon Peak production layout.*

collected and placed on the ground and allowed to cool at ambient air temperatures to better simulate conveyor cooling. Three preforms are collected in order to air cool: one from the front, the middle, and the back/rear of the shell. The middle air-cooled preform and the quenched preform are usually sequentially formed preforms.

The entire production system, not just the PRM, needs to be setup and verified before any product can be produced or any meaningful data can be collected. This includes setting up and verifying: the billet size, the billet temperature upon exiting the induction heater, the pierced shell dimensions, and the final product quality. The size of the billets to be used is verified by manually measuring the outside diameter (OD) with calipers. Only a random sampling is conducted, since the billets are supplied internally and have already been tested to ensure they are within the specification limits. The billet temperature upon exiting the induction heater is measured with an optical pyrometer, and displayed in the piercing mill pulpit. During setup only, this temperature reading is also verified by using a HotShot™ temperature sensor gun.

Since it is difficult to measure either the inside diameter (ID) or wall thickness of the shell at such high temperatures, the DVG sensor system measures the OD (D_1) and length (L_1) dimensions of the billet prior to piercing, so that the shell dimensions can be calculated.[1] Assuming that no material is lost during the piercing process, the volumes of the billet and the shell are equal. By using optical sensors to measure the length (L_2) and average OD (D_2) of the shell, the shell ID (d_2) and wall thickness (w) can be calculated, as shown in Equations 2.1 and 2.2. Prior to the experiment, multiple shells are measured with calipers to verify the DVG system within 0.5 mm. These shells are collected on the cooling bed because they have cooled too much to be formed after the caliper inspection.

$$d_2 = \sqrt{D_2^2 - \frac{D_1^2 \times L_1}{L_2}} \tag{2.1}$$

$$w = \left(\frac{D_2 - d_2}{2} \right) \tag{2.2}$$

2.2. Profile Ring Mill Concept

The new PRM technology is the most recent attempt to improve the manufacturing process of preforms for bearing assembly components. Instead of cutting a part from a finished tube, the PRM reduces the cycle time per piece by continuously forming preforms directly from a shell that has only been pierced, but not finished. The shell enters the PRM between three forming rolls that are turning in unison with a mandrel inserted inside the shell, as shown in Figure 2.2. The mandrel is responsible for producing the constant ID, and the forming rolls are responsible for forming the profile on the OD and separating the preforms into distinct pieces, as shown in Figure 2.3.

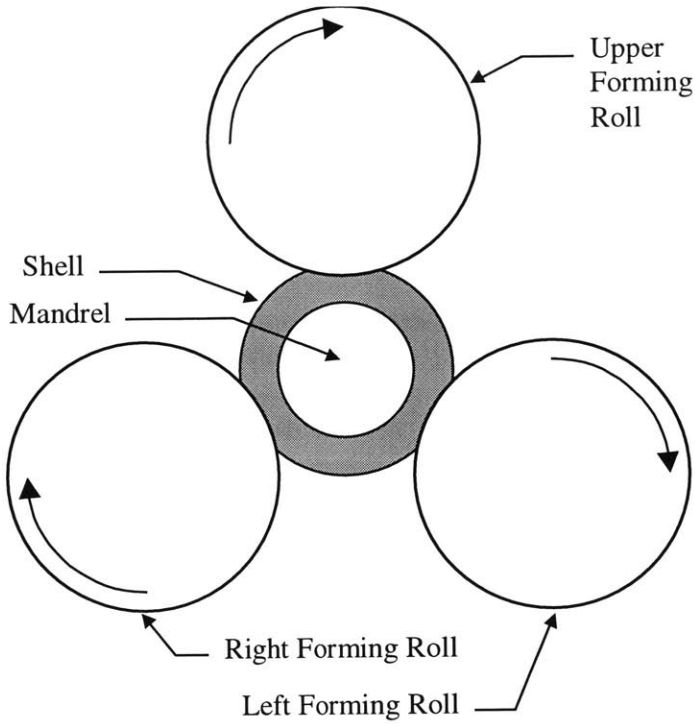

Figure 2.2. *Schematic end view of PRM from exit side. (Flow is out of page.)*

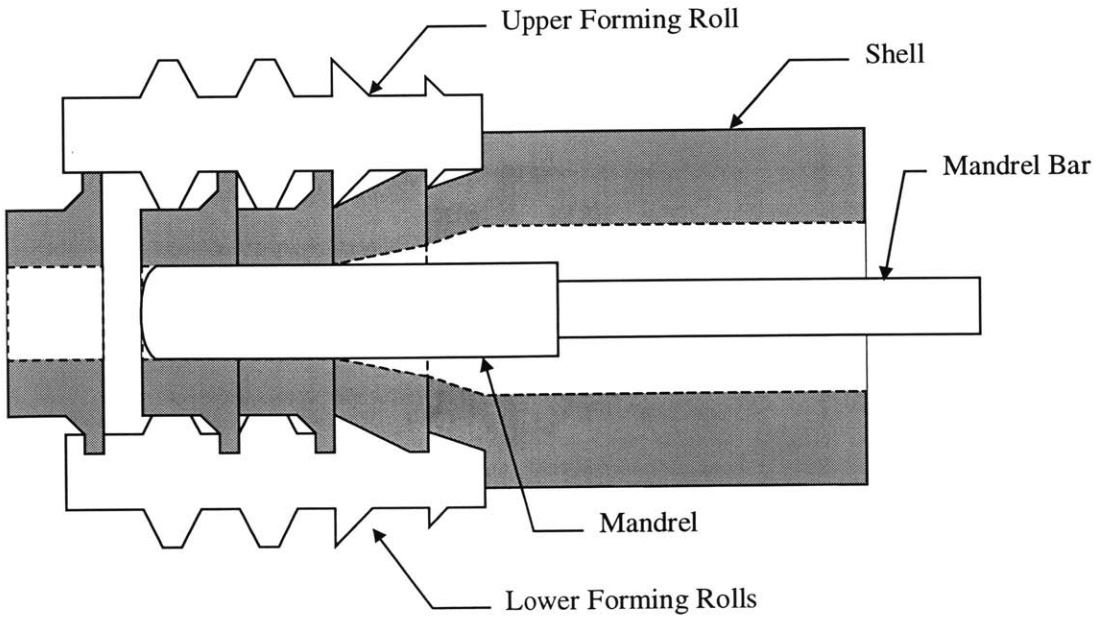

Figure 2.3. *Schematic side cross-sectional view of PRM. (Flow is right to left.)*

As one part forms, the unused material is not scrapped, but instead it is used to form the next part, as shown in Figure 2.4. Since some of the material required to form each part is provided by the surrounding parts, it is not surprising that a couple of the preforms at the front and rear of the shell do not form completely and must be scrapped at the exit of the PRM. This is one reason why the PRM is capable of processing a pierced shell. Since the end pieces must be scrapped, it is not important that the ends of the pierced shell are imperfect. Also, variation in the size of the incoming shell is acceptable, since the shell will be reduced to the size of the desired preform, as shown in Figure 2.3.

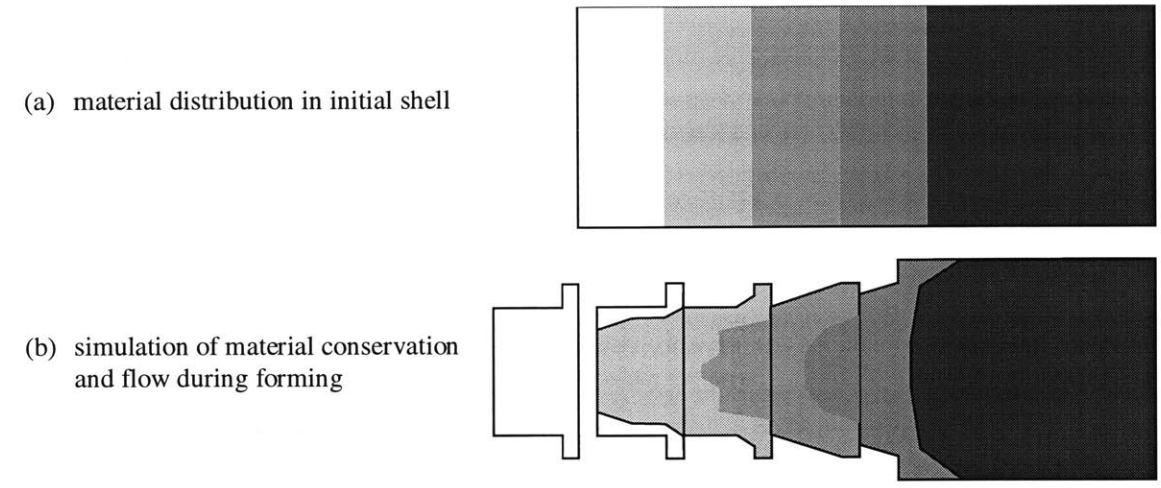

Figure 2.4. *Schematic of material f low during forming.*

2.3. Machine Parameters

The PRM requires part specific tooling, and each set of tooling may operate at different settings. Therefore, in order for the mill to function properly, it is crucial that all three forming rolls be properly setup and aligned to the center-point. Figure 2.5 illustrates the important setting parameters for the forming rolls. The feed angle (α) is the rotation of the forming rolls about their radial axis. All three forming rolls must have the same feed angle ($\alpha_1=\alpha_2=\alpha_3$). When the

feed angle is 0°, the rolls are simply parallel to the shell, but as the feed angle is changed, the rolls become skewed in relation to the shell. The gorge is the radial distance from the center-point of the PRM to the surface of the forming rolls. (Or the radius of the circle that circumscribes all three rolls.) As with the feed angle, the gorge must be the same for all three rolls. Any differences in the setting of the three forming rolls may produce significant part defects or prevent the mill from operating at all.

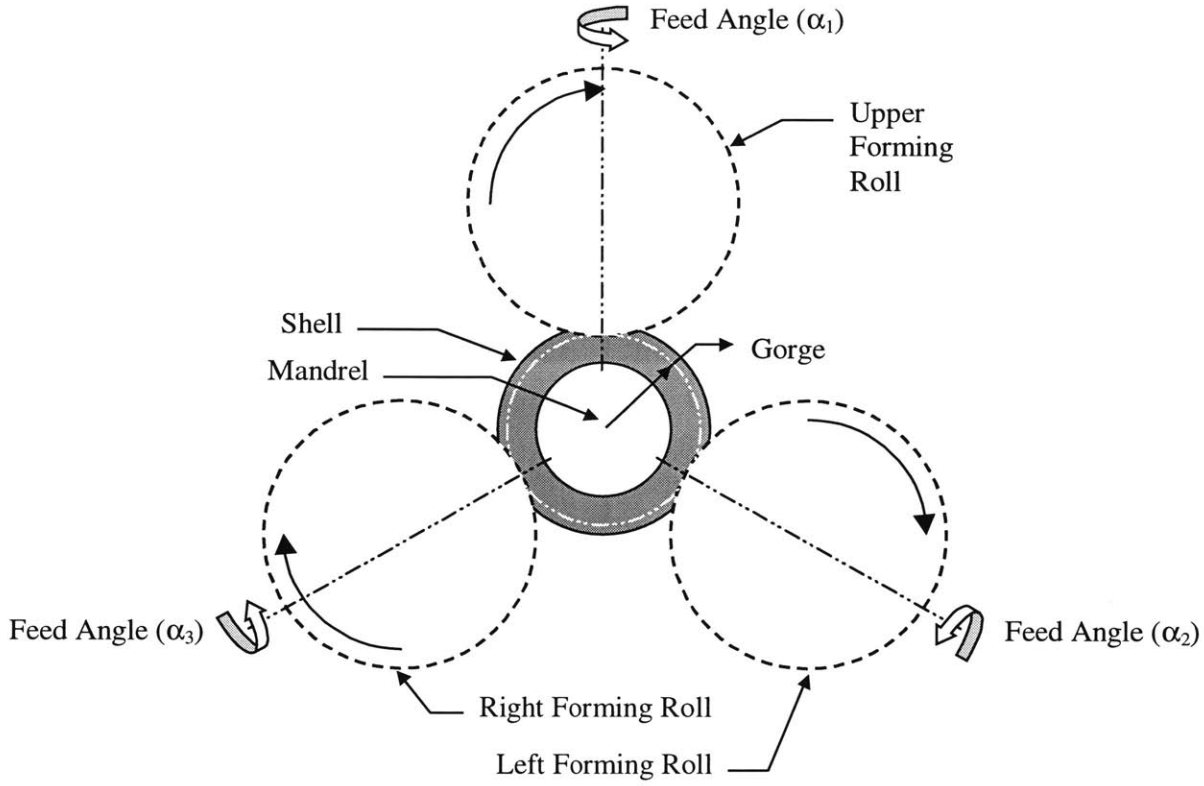

Figure 2.5. *Schematic end view from exit side of important PRM setting parameters. (Flow is out of page.)*

It is equally important that the mandrel be properly setup. Figure 2.6 illustrates the key setting parameters for the mandrel. The lead is the horizontal distance from the end of the mandrel tip, to the end of the forming rolls. All three rolls must have the same horizontal alignment. The gap size is the distance between the pierced shell ID and the mandrel OD. The gap size should always be greater than zero, or the mandrel will not fit inside the shell.

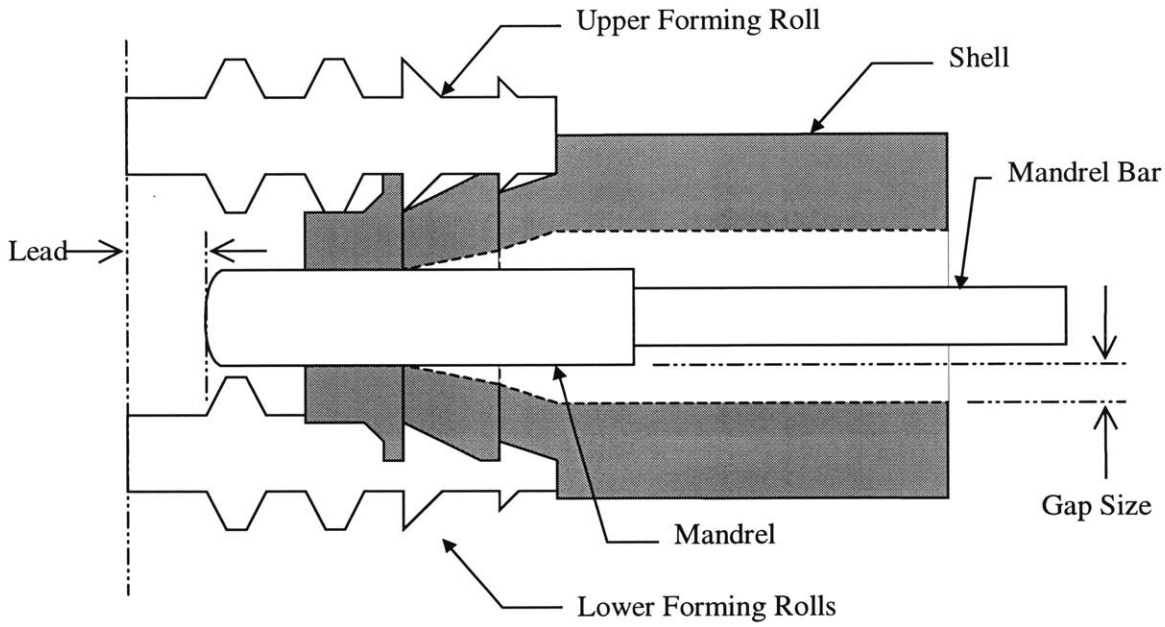

Figure 2.6. *Schematic cross-sectional side view of important PRM parameter settings. (Flows is right to left.)*

The settings will not only vary between parts, but they may also vary between different tooling sets for the same part.

2.4. Important Product Attributes

2.4.1. Defined Dimensions

For each preform, there are specifications for both dimensions and surface defects. As shown in Figure 2.7, there are seven dimensions with specific tolerances: (A) the small rib OD, SROD; (B) the large rib OD, LROD; (C) the OA width, OAW; (D) the rib width, RIB; (E) the wall thickness, WALL; (F) the large rib ID, LRID; and (G) the small rib ID, SRID. The preform specifications include tolerances for both the average size and the total indicated run out for each dimension.

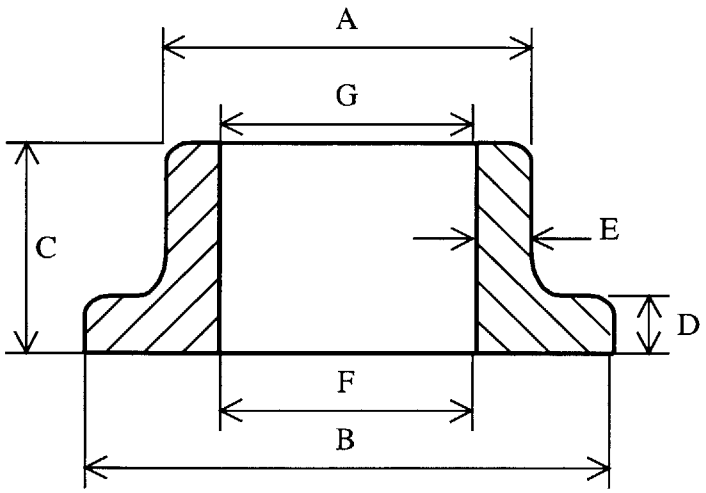

Figure 2.7. *Critical preform dimensions.*

Once the preforms collected for sampling have cooled (See Section 2.1), they require gauging to measure their dimensions. Timken uses direct contact digital gauges to measure the preforms and the software program, ASI, to analyze and automatically record the data. Each preform is manually rotated in the gauge to measure the entire part. (Depending on the feature it will require a minimum rotation from 90° to 360°.) As the preform moves against the contact,

the contact also moves, causing a change in the internal resistance of the gauge, which is then related to a distance and displayed as the displacement of the contact. Each gauge is calibrated on a regular basis, using a "master" part that is within 0.001" of the specification to verify that a zero reading represents the target size.

Each gauge is capable of three readings: minimum, maximum, and dynamic. Since the dynamic reading represents the current reading, the dynamic reading recorded is the last reading before the preform is removed from the gauge. The average product sizes (size) and the total indicated run-out (TIR) can be calculated directly from the gauge output:

$$TIR = Maximum - Minimum \tag{2.3}$$

$$Size = \left(\frac{Maximum + Minimum}{2} \right) \tag{2.4}$$

The gauges are extremely sensitive and require practiced use in order to provide accurate and useful measurements. Improper calibration of the gauges will also result in skewed measurements. While an under-rotation will result in an incomplete sampling of the part, the only problem caused by an over-rotation is an increase in the possibility of operator error. If the part is allowed to shake in the gauge, then the TIR recorded will be higher than the actual TIR, and the size of the part may also be incorrectly recorded. Sometimes, the part may have sustained sufficient damage to prevent it from being inserted into the gauge and properly measured. It is also possible that the part may be so far out of specification that a reading is not registered. Such cases are recorded in ASI as a non-entry.

2.4.2. Common Surface Defects

Since the PRM produces preforms, there is some extra material (stock) designed into the preform specifications. Therefore, the depth of the surface defects must be less than the stock that will be removed during subsequent machining processes. There are two common types of surface defects that are encountered: lapping on the OD and underfill on the ID, as shown in Figure 2.8. Many defects are not visible because they are smaller than 0.020". Therefore, it is crucial to be careful when handling the samples, since any slight disturbance could greatly influence defects.

There is a lot of time and resources required to examine the entire surface for defects. Therefore, after surveying the part for the most likely defect location, one surface point is selected for analysis. The sources of defects are visible, even when the defects themselves are not. Since the worst defects are associated with lapping, the location that appears to have the worst lapping effects is selected for microanalysis.

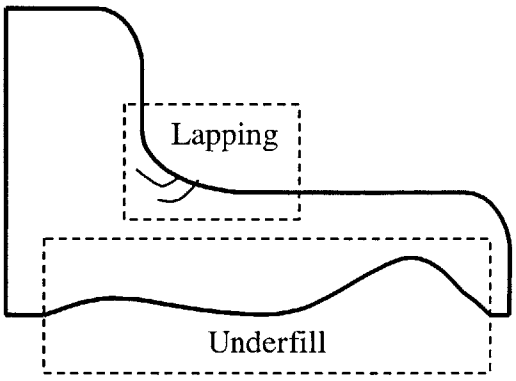

Figure 2.8. *Schematic of common preform surface defects*

Once the desired surface has been determined, a sample slice obtained by using a carbide saw is mounted in a plastic and polyester resin. After the resin has set, the sample is ground on

an automatic grinding stone and then manually polished with a series of polycrystalline diamond sprays, decreasing from a 15-micron solution down to a 1-micron solution. The sample is also rinsed in ethyl alcohol to prevent rusting during storage after the analysis. To ensure that there is a clear picture of the surface during viewing under a microscope, the surface is flattened with a vice.

A light microscope is used to examine the desired sample surface. The sample is manually moved under the lens until the entire surface has been investigated. When a defect is detected, a picture of the exact view through the microscope lens is taken with any regular camera. Pictures are taken of all the defects found in each sample. The magnification level and defect location are recorded on each picture taken. The defect characteristics can be measured with a ruler, and the actual surface defect can then be calculated:

$$Actual = \frac{RulerMeasurement}{Magnification} \tag{2.5}$$

It is not necessary to measure all of the laps identified in each area since only the maximum defect is important. The lap depth is measured as the maximum perpendicular distance from a point on the lap to the desired surface datum (the datum tangent to the desired surface), as shown in Figure 2.9. Often when lapping occurs, it is accompanied by a divot and results in the creation of a defect. Since some material will be removed from the surface during the green machining process, the severity of the defect depends on the desired surface datum, and not on these surface blemishes. If there is no underfill, then the desired surface datum is the surface viewed.

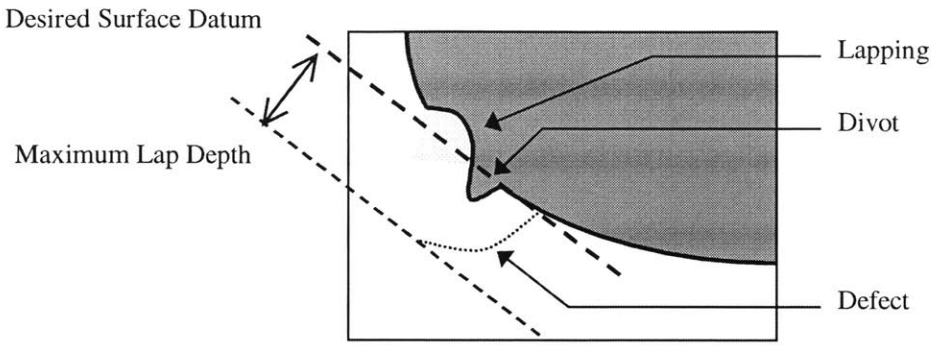

Figure 2.9. *Schematic of maximum lap depth measurement.*

The ID underfill is the lack of material on the ID. The depth is the perpendicular distance from the desired surface datum to the actual surface datum (the datum parallel to the desired surface datum through the extreme point on the surface underfill), as shown in Figure 2.10. Only the maximum distance needs to be recorded though. The width of the maximum ID underfill can also be determined as the distance along the desired surface datum from where the underfill begins to where it ends.

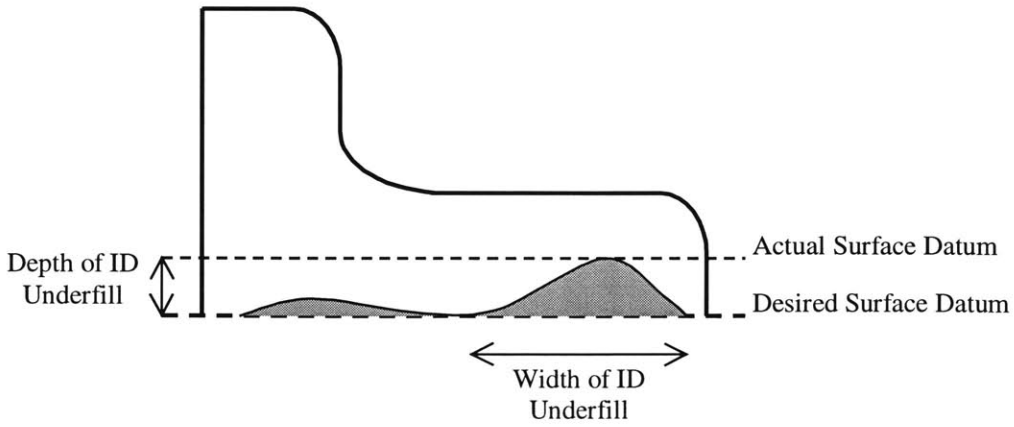

Figure 2.10. *Schematic of ID underfill measurement.*

Chapter 3: Theoretical Investigation

3.1. Objective

There are many important factors that may affect the successful operation of the PRM, such as the shell characteristics, the tooling settings, and the physics of the PRM design.[1] Since the PRM is a complex three-dimensional process, the relationships between these factors are not trivial. While the shell characteristics and tool settings can be adjusted relatively easily, the basic physics of the PRM forming process cannot be changed. Although, the gorge contributes to defining the final size of the product, there are other factors, such as elastic recovery and shrinkage, that also affect the product even after leaving the PRM. Therefore, in order to control the attributes of the final product, these additional factors must be related to the other parameters of the PRM. By understanding the post-forming factors and analyzing the importance of the shell characteristics on the basic PRM physics, direct relationships can be derived to relate the product size to the PRM settings. These relationships make it possible to trace the root cause of the DVAL to the forming temperature.

3.2. Temperature

The material temperature during the forming process is a critical input parameter. Unfortunately, the PRM design does not allow for easy monitoring of the material temperature in the forming zone. Therefore, since the forming temperature can not be measured directly, an alternative method must be developed to approximate the forming temperature. The last opportunity to directly monitor the material temperature occurs when a pierced shell is laying on the inlet table just prior to entering the PRM. The standard process for measuring the temperature

of hot steel in production is to use an optical pyrometer. As the temperature of steel increases, the color of the steel changes from dark red, to bright orange, and finally to bright yellow. The optical pyrometer translates the wavelength of the color emitted from the steel into a temperature reading.

3.2.1. Maximum Shell Temperature (MST) Method

Since the exact forming temperature could not be determined, the original approximation required aiming an optical pyrometer at the approximate middle of the shell as it lay on the entry table before entering the forming mill. Since the computer database requires a single entry, the maximum temperature was recorded and entered into the database. Assuming that this maximum shell temperature was characteristic of the overall shell temperature, it was then used to represent the forming temperature.

This model assumes that any two shells with the same maximum temperature recorded will have the same forming temperature, however this assumption is not necessarily true. By choosing to use the maximum temperature over a range of time and shell locations, instead of the temperature at one specific location, it was recognized that a temperature variation along the shell length existed. The maximum shell temperature model disregards the importance of the temperature profile within a shell.

3.2.2. Conventional Shell Temperature Profile (STP) Model

It is common that the temperature of a hot pierced shell is non-uniform. At the Tryon Peak plant, the front of the billet exits the induction furnace before the back of the billet. Since the billet begins cooling once it is exposed to the ambient air, the front of the billet is cooler than

the back of the billet at any given point in time. During the billet piercing process, the front of the billet is pierced open first. Since the geometry of a hollow shell results in a faster rate of cooling than the geometry of a solid billet, the rate of cooling for the front of the shell will be faster than that of the back of the shell during the piercing process. Therefore, the shell temperature differential is even greater than the billet temperature differential.

The shell temperature profile model proposes that the forming temperature profile is similar to the shell temperature profile. The fundamental problem with this theory is that the definitions of the two profiles address different parameters. The shell temperature profile relates temperature to shell location at a specific point in time, but the forming temperature profile relates temperature to time at a specific location--the forming zone. This model would be sufficient if the shell temperature remained constant or if the entire shell was formed at once, but neither of these scenarios holds true. While the shell temperature profile model takes variation into account, it fails to account for the radiant cooling of the rear of the shell while the front of the shell is formed.

3.2.3. Proposed Entry Temperature Profile (ETP) Model

Since the shell temperature is over 1800°F, it is not surprising that the shell cools rapidly. Indeed, the entire shell is cooling while it lies on the inlet table. When the front of the shell begins forming, it is close to the temperature predicted by the Shell Temperature Profile model, but the remainder of the shell remains exposed to the ambient air and continues cooling. The STP model failed to take into account this cooling effect. The ETP model accounts for both shell cooling and variation along the shell length by focusing on variation by time at a specific

location. As shown in Figure 3.1, a simple model of the shell at one specific location can be used to predict the effects of the radiant cooling.

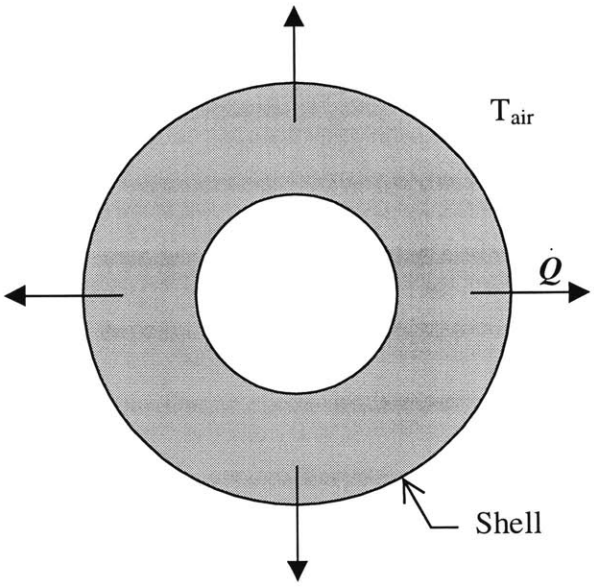

Figure 3.1. *Model for radiant cooling effects of shell prior to PRM*

There are several assumptions made by this simple model. One assumption is that the air temperature, T_{air}, remains constant around the entire shell. Also, the rate of cooling is considered to be uniform around the entire surface, even though the bottom of the shell is resting in a trough and is less exposed to the air. The most significant assumption is that the adiabatic heating resulting from the work performed by the rolls is considered negligible.[2] From this simple model, the cooling rate, Q, can be related to the shell temperature, T:

$$\dot{Q} = \sigma_{SBC} \times \varepsilon \times A_{surf} \times \left(T^4 - T_{air}^4\right) \tag{3.1}$$

where ε is the material thermal diffusivity, A_{surf} is the surface area, and the Stephan-Boltzman constant *is* $\sigma_{SBC}=0.174x10^{-8}\ B\ hr^{-1}\ ft^{-2}\ R^{-4}$.

The cooling rate is fastest at higher temperatures. Also, since the cooling rate decreases as the temperature decreases, if two objects begin at different temperatures, the difference in the two temperatures will decrease over time. This relationship can be used to estimate the temperature at either the time of forming, or mill entry, by simply changing the length of time the shell is cooling. Since the material moves at a constant rate through the machine, all material will cool for an equal amount of time in the same surrounding conditions between the point of mill entry and the forming zone. The only effect on the cooling rate that is changing during this period is the decreasing material temperature. Therefore, any variation in the mill entry temperature will be slightly greater than the temperature variation at the time of forming.

3.3. Material Flow Stress

The material flow stress represents the material's malleability, or resistance to forming. As the flow stress increases, the material becomes less malleable and more difficult to form. Timken has derived a relationship for the material flow stress, σ, of hot steels as:

$$\sigma = \sigma(d_o, \varepsilon, T) \tag{3.2}$$

where d_o is the grain size, ε is the strain rate, and T is the material temperature.[3] The grain size and the strain rate are dependent on the grade of steel and the design of the preform and tooling, respectively. Therefore, they may be assumed to remain constant throughout the entire forming process of one shell, and also for any other shell of the same size for the same part and the same

tooling set. Also, by focusing on only a narrow range of high temperatures, Equation 3.2 can be reduced to a simple linear relationship. Therefore, the material forming temperature can be directly related to the material flow stress, as:

$$\sigma \approx b_{\sigma T} - \left(k_{\sigma T} \cdot T\right) \tag{3.3}$$

where $k_{\sigma T}$ and $b_{\sigma T}$ are both positive constants, dependent on the grain size, the strain rate, and other natural constants. Although, these values remain constant throughout any one process, they may vary depending on the part and the machine settings. The four combinations of the maximum and minimum grain size and strain rate represent the extreme scenarios for the entire range of values possible on the PRM, as shown in Figure 3.2. The corresponding constants are shown in Table 3.1.

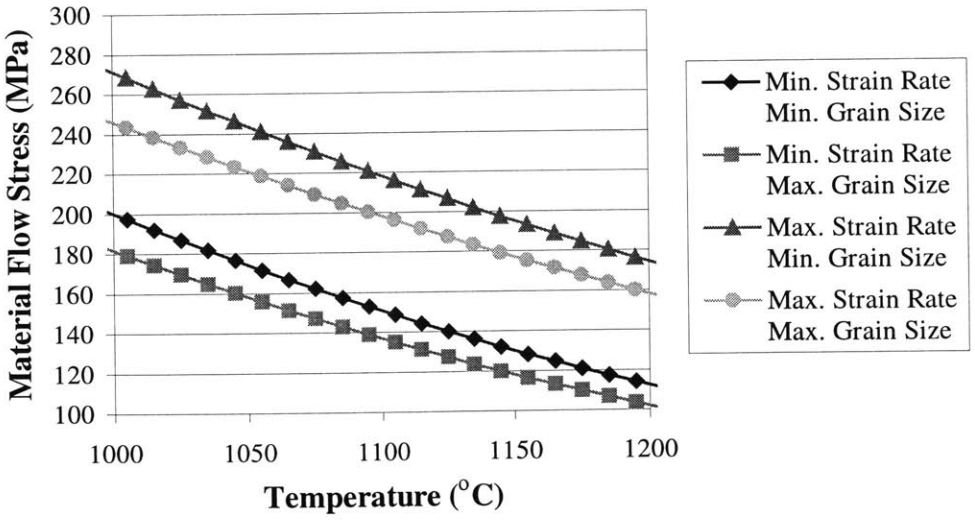

Figure 3.2. *Material temperature versus flow stress for entire range of possible material properties.*

Table 3.1. *Process constants for the four extreme PRM possibilities.*

Strain Rate	Grain Size	$k_{\sigma T}$	$b_{\sigma T}$	$b_{\sigma T}/k_{\sigma T}$
		MPa°F	MPa	°F
Minimum	**Minimum**	0.25	650	2600
Minimum	**Maximum**	0.23	600	2609
Maximum	**Minimum**	0.27	750	2779
Maximum	**Maximum**	0.25	700	2800

Equation 3.3 can be further derived to determine a relationship between the change in temperature, ΔT, and the corresponding flow stress change, $\Delta\sigma$, as:

$$\Delta\sigma \approx -k_{\sigma T} \times \Delta T \tag{3.4}$$

This identifies the negative linear relationship between the material flow stress variation and the material forming temperature variation. While the magnitude of the change in the material flow stress is important, the relative effect of this variation is of even greater relevance. The significance can be obtained by calculating the percentage change of the material flow stress variation, $\Delta\sigma^*$, defined as:

$$\Delta\sigma^* = \frac{\sigma_2 - \sigma_o}{\sigma_o} = \frac{\Delta\sigma}{\sigma_o} \tag{3.5}$$

By substituting Equation 3.4 into Equation 3.5 for the change in flow stress, and then substituting Equation 3.3 in place of the initial flow stress, σ_o, the percentage change of the material flow stress may be derived further, as:

$$\Delta\sigma^* \approx \frac{\Delta T}{T_0 - \frac{b_{\sigma T}}{k_{\sigma T}}} \tag{3.6}$$

This highlights the dual importance of the forming temperature. Not only does a large temperature range, ΔT, cause significant material flow stress variation, but a decrease in the actual magnitude of the temperature itself, T_o, also increases the material flow stress variation. Therefore, in order to reduce material flow stress variation, it is not only important to maintain a constant temperature, but also a high temperature. Of course, if there is no temperature variation, then there is no material flow stress variation, regardless of the magnitude of the temperature.

3.4. Basic PRM Physics

The PRM relies upon the basic concept that steel is easier to work at higher temperatures. The amount of work, W, required to deform the shell is directly related to the force exerted by the forming rolls, F, and the distance over which that force is exerted, D, as:

$$W = F \times D \tag{3.7}$$

For parts with a profiled OD, the distance that must be worked varies from the front to the back of each piece, but remains the same from piece to piece. Therefore, the distance may be considered constant for any given part.

The material flow stress represents the material's malleability, or ability to be worked. A material with a higher flow stress requires more work to deform the material by the same amount. Therefore the flow stress is also directly related to the forming force. Although many models have been developed to relate force and flow stress for simple two roll deformation

processes, modeling this relationship in the PRM is extremely difficult because there are three rolls and a non-uniform forming roll diameter.[4] Nonetheless, the basic relationship still exists and the required force can be directly related to the flow stress, as:

$$F \approx k_{F\sigma} \times \sigma \tag{3.8}$$

where $k_{F\sigma}$ is a positive constant.

While an increase in the material flow stress requires an increase in the amount of work exerted in order to maintain the same deformation, work can not be simply performed, it must be supplied from a power source. The forming rolls draw their power from an electrical source. Therefore, the amount of power, P_s, supplied is directly related to the current, I, and the voltage, V, supplied to the PRM, as:

$$P_s \approx V \times I \tag{3.9}$$

Since the voltage remains constant, the only method of increasing the power supplied is an increase in the current supplied.

Since work and power are related by the amount of time, t, that the power is supplied, as shown in Equation 3.10, by substituting Equations 3.7 and 3.9 into Equation 3.10, a direct relationship between the current and the roll force can be derived, as:

$$W = P_s \times t \tag{3.10}$$

$$\frac{F}{t} \approx \frac{I \times V}{D} \tag{3.11}$$

This relationship shows that for a given system at a given period in time, an increase in the current supplied will result in an increase in the force exerted, and vice versa. This is useful for the PRM since at this time the current, and not the exerted force, can be continuously monitored.

The gorge is adjusted by an adjustable screw thread. Once the gorge is established, the forming rolls are locked in place by a pneumatic cylinder. This is done to make the PRM as rigid as possible. Nevertheless, the roll forces experienced by the PRM are on the order of 20,000 lbs. If the PRM's rigidity is insufficient, then as the roll forces increase, the forming rolls will be able to move radially outwards, effectively increasing the gorge. While establishing an exact relation is difficult, the forming force can be directly related to the gorge, G, as:

$$G \approx k_{gs} + (k_{GF} \cdot F) \tag{3.12}$$

where k_{GF} is a positive constant and k_{gs} is the actual gorge setting.

3.5. Final Product Size and Variation Along Shell Length (DVAL)

It appears that the gorge and the final product size should be equal by definition. This is not true, however, because of the various post-forming phenomenon that take place. Therefore, the final product size, S, can be related to the gorge by a scaling factor, Φ, that accounts for these phenomenon, as:

$$S = \Phi \times G \tag{3.13}$$

By definition, Φ is always greater than zero, and if no post-forming effects exist, then Φ equals 1. Therefore, by combining the previous equations, the size can be related to the forming temperature, T, as:

$$S = \Phi \cdot \left[\left(k_{gs} + b_{\sigma T} k_{GF} k_{F\sigma} \right) - \left(k_{GF} k_{F\sigma} k_{\sigma T} \right) \cdot T \right] \tag{3.14}$$

While this relationship appears to be rather complicated, it is actually quite simple. Since all of the constants are non-negative, and Φ is greater than zero, as the temperature increases, the size of the final product will decrease. Likewise, as the temperature decreases, the product size will increase. The magnitude of the decrease is dependent on the magnitude of the various constants related to the design of the PRM.

Dimensional variation along the shell length, DVAL, can easily be defined as the change in size. Therefore, by using Equation 3.14, the DVAL can be related to the forming temperature and post-forming phenomenon, as:

$$DVAL = S_2 - S_0 = \underbrace{\left(\Phi_2 - \Phi_1 \right) \left(k_{gs} + b_{\sigma T} k_{GF} k_{F\sigma} \right)}_{External} - \underbrace{\left(k_{GF} k_{F\sigma} k_{\sigma T} \right) \left(\Phi_2 T_2 - \Phi_1 T_1 \right)}_{Internal} \tag{3.15}$$

While this relationship appears even more complex than our relationship for the size of the parts, it can be viewed simply as having two factors: internal and external. Therefore the DVAL will exist unless both factors are equal. While it is possible that this occurs when both factors are non-zero, the complexity of the PRM makes this very unlikely. Therefore, it may be assumed that the DVAL will only be zero if both the internal and external factors equal zero.

Since k_{gs} is non-zero, the term of constants in the external factor will always be non-zero. Therefore, the external factor will be zero, if, and only if, the post-forming phenomenon is non-existent or constant. In order for the internal factor to be zero, either one of the constants must be zero, or the temperature and post-forming phenomenon relationship must be zero. The constant $k_{F\sigma}$ can not be non-zero, because then roll force would always be zero, and this is not feasible. Also, since Equation 3.3 was derived from actual testing, the constant $k_{\sigma T}$ has been proved to be non-zero. Perhaps for certain operating ranges these two constants may be reduced to minimal levels, but in the current operating range of the PRM they will always be non-zero. Therefore, in order for the internal factor to be zero, either k_{FG} must equal zero, or both the temperature and the post-forming phenomenon must be constant. As a result, there are two conditions that must be met in order for the DVAL to be zero:

$$\begin{aligned} &\text{Condition1}: \Phi = constant \\ &\text{Condition2}: \begin{cases} k_{GF} = 0 \\ \quad or \\ \Phi, T = constant \end{cases} \end{aligned} \tag{3.16}$$

3.6. Gorge Swelling

The constant k_{FG} was created to account for the possible "gorge swelling" as a result of large roll forces. By definition, k_{FG} will be non-zero as long as swelling exists, but if the swelling effect does not exist, then k_{FG} will be equal to zero. In order for gorge swelling to be the only factor that results in DVAL, then Condition 1 requires that Φ must be constant, and condition 2 requires that the temperature must be non-constant. (If the temperature was constant, then the

DVAL would equal zero, regardless of the possibility of gorge swelling.) Therefore, evaluating Equation 3.15 will produce the DVAL caused by swelling, $DVAL_{sw}$, as:

$$DVAL_{sw} = -(k_{GF} k_{F\sigma} k_{\sigma T}) \Delta T \tag{3.17}$$

3.7. Product Shrinkage

As the preforms cool after forming, the internal microstructure changes. The exact microstructure that forms is dependent on the rate of cooling. The microstructure becomes denser the longer the preform cools. As a result, the preform "shrinks" as it cools and becomes smaller than the hot preform. The preforms cool by radiant effects in the same manner as the shell cools on the entry table. As expressed by Equation 3.1, the rate of cooling is dependent on the material temperature. Therefore, the scaling factor is negatively related to the temperature, as:

$$\Phi = -\Phi_{sh} \times T \tag{3.18}$$

where the shrinkage factor, Φ_{sh}, is a non-negative number. Since temperature variations will result in a non-constant Φ, k_{FG} must equal zero in order to satisfy Condition 2. Condition 1, however, cannot be satisfied. Therefore, evaluating Equation 3.15 will produce the DVAL caused by shrinkage, $DVAL_{sh}$, as:

$$DVAL_{sh} = -(k_{gs} \Phi_{sh}) \Delta T \tag{3.19}$$

3.8. Elastic Recovery (Springback)

Instead of maintaining the shape defined by the forming rolls, once the preform exits the PRM it "springs back" towards its initial shape, the pre-formed shell. Elastic recovery is a

common problem during forming processes.[5] The material yield stress is one of the key components of elastic recovery. As the material yield stress increases, the range of the elastic domain is increased and the magnitude of the springback is increased. The material yield stress has an inverse relationship with temperature in a similar manner as the material flow stress. As the temperature decreases, the material yield stress increases, and vice versa. Therefore, the scaling factor is positively related to the stress, as:

$$\Phi = \Phi_{sp} \times \sigma \tag{3.20}$$

where the springback factor, Φ_{sp}, is a non-negative number. Since stress variations will result in a non-constant Φ, k_{FG} must equal zero in order to satisfy Condition 2. Condition 1, however, cannot be satisfied. Therefore, evaluating Equation 3.15 will produce the DVAL caused by springback, $DVAL_{sp}$, as:

$$DVAL_{sp} = -\left(k_{\sigma T} k_{gs} \Phi_{sp}\right) \Delta T \tag{3.21}$$

3.9. Proposed Theoretical Explanation

The PRM operates on the fundamental theory that the material properties are dependent on the forming temperature. While there are advantages to having high forming temperatures, there can also be disadvantages if the temperature is not carefully controlled. The temperature directly affects the final product size, as stated in Equation 3.14. The proposed entry temperature profile (ETP) model incorporates radiant cooling into the previous shell temperature profile (STP) model to improve the approximation of the forming temperature. Unlike the other parameters that affect the final product size, the improved ETP model predicts a significant

decrease in the forming temperature during the forming process as a result of the radiant cooling that the exposed rear of the shell undergoes. This temperature variation results in a significant DVAL, as stated in Equation 3.15. The temperature is related to other factors of DVAL as well: gorge welling, shrinkage, and elastic recovery. In every case, the decrease in the forming temperature predicted by the ETP model results in an increase in the final product size. Also, given the same temperature variation, the DVAL will increase at lower temperatures.

Chapter 4: Experimental Investigation

4.1. Identification of Dimensional Variation

When production first began, there were concerns about surface defects and dimensional tolerances, but it was assumed that all of the preforms produced from each shell were essentially the same. Therefore, a shell's preforms were usually characterized by averaging three samples, one from the front, middle and rear (FMR). With this approach, any dimensional variation in the product was not recognized. The problem of DVAL finally became apparent when, instead of just viewing the averages, the data from prior experiments was analyzed in its entirety.

4.1.1. Design of Experiments (DOE)

Following the standard operating procedure, a series of design of experiments (DOE) was conducted on the PRM in Tryon Peak to investigate the relationships between various parameters. A set of FMR samples was collected, measured, and microanalyzed for each shell produced. While the first three DOE provided the expected, valuable information about the relationships of the PRM settings and the final product, the fourth DOE (DOE4) provided some additional and unexpected results. There were eighteen shells formed during DOE4, which addressed lead and feed angle for the 9-add part, which is a typical part with a 2.5" OD. (See Appendix A for complete DOE4 test data.) Since the product was assumed to be uniform for any given shell, the average of the three samples was considered sufficient to represent an entire shell. This assumption can be explored by plotting the SROD size for all three locations for each shell on the same graph, as shown in Figure 4.1.

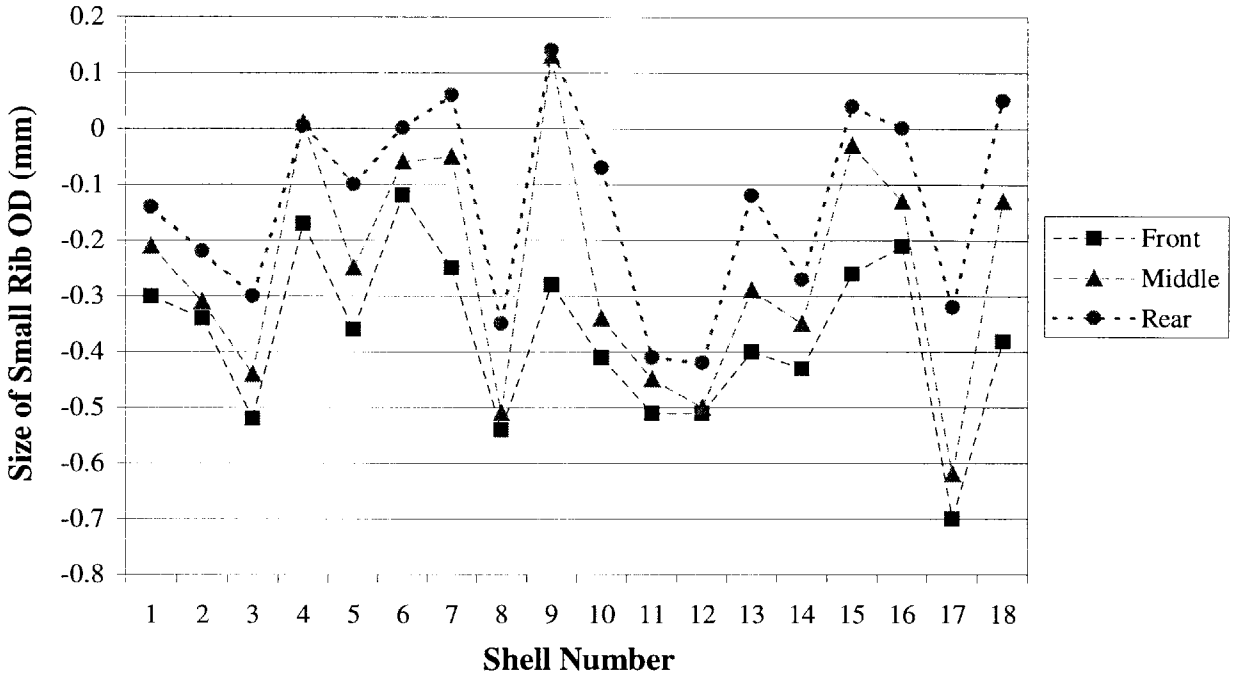

Figure 4.1. *Small rib OD size versus shell location in DOE4.*

For every shell, the rear sample is the largest and the front sample is the smallest. The difference in size ranges from 0.10 mm to 0.40 mm. This is a significant percentage of the entire tolerance range of 1.0 mm. Similar variations were noted in the other dimensions as well. Some variation in the magnitudes and linearity of the DVAL in each shell is to be expected, since the exact location of the samples collected is dependent on the collecting operator. In addition, it is not important that the settings were not the same for each shell run, because the same trend of variation is clear in every case.

It is also important to investigate whether or not the surface defects are uniform along the length. This can be achieved by plotting all three locations on the same figure for the maximum defect depth, as shown in Figure 4.2.

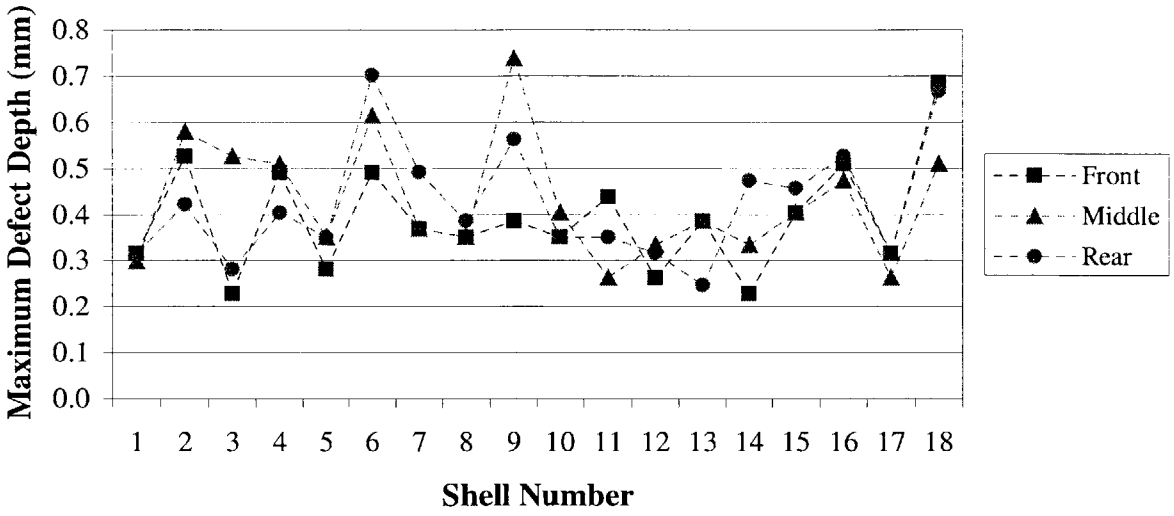

Figure 4.2. *Maximum defect depth versus shell location in DOE4.*

There does not appear to be any systematic variation in the maximum defect depth with regard to the position of the preform along the shell. Sometimes the front sample is the worst, and sometimes the front sample is the best. The initial assumption that the entire product from each shell was uniform does not appear to hold. While the surface defects do not appear to be related to the shell position, there does appear to be a consistent and significant increase in the product size from the front of the shell towards the rear of the shell.

4.1.2. Whole Shell Test

Although the DVAL was identified in the DOE4 analysis, the cause and severity of the problem remained unclear. The standard FMR sampling did not provide sufficient data to investigate the problem adequately. Therefore, it was necessary to collect a complete set of data for an entire shell. All of the preforms from one shell were collected and measured for two typical parts: the 9-add part with a 2.5" OD, and the 7-add part with a 2.0" OD. (See Appendix

B for complete test data.) The small rib OD sizes for the 9-add preforms are shown in Figure 4.3 in sequential order. A linear trendline was fit to the data using Microsoft Excel to determine the dimensional variation per piece.[1]

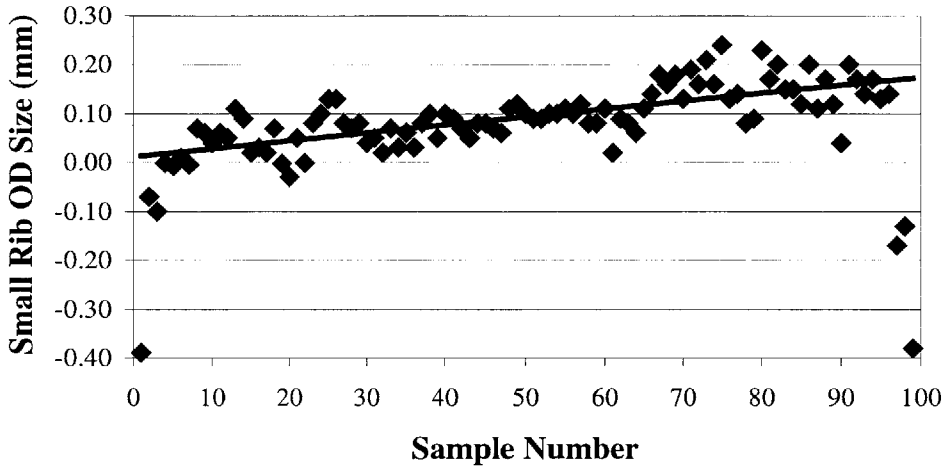

Figure 4.3. *Small rib OD size in order of production for 9-add whole shell test.*

The total dimensional variation along the shell length was calculated for each dimension by multiplying the slope of the trendline by the number of preforms, as shown in Table 4.1.

Table 4.1: *Total dimensional variation along shell length (DVAL) for whole shell tests.*
(Note: * = non-linear variation, n/a = insignificant variation)

Type	Dimension	Units	9-add	7-add
Size	OD - Small Rib	mm	0.170	0.253*
	OD – Large Rib	mm	0.200	0.276
	ID – Small Rib	mm	0.362	0.315
	ID – Large Rib	mm	0.451	0.426
	Width – Overall	mm	0.059	0.214*
	Width – Rib	mm	0.020	0.074
TIR	OD – Small Rib	mm	0.209	n/a
	OD – Large Rib	mm	0.253	n/a
	ID – Small Rib	mm	0.266	n/a
	ID – Large Rib	mm	0.274	0.092
	Width – Overall	mm	0.038	n/a
	Width – Rib	mm	n/a	n/a

In addition to gauging every preform, 18 samples from the 9-add shell were microanalyzed for surface defects, as shown in Figure 4.4. (See Appendix B for complete data.)

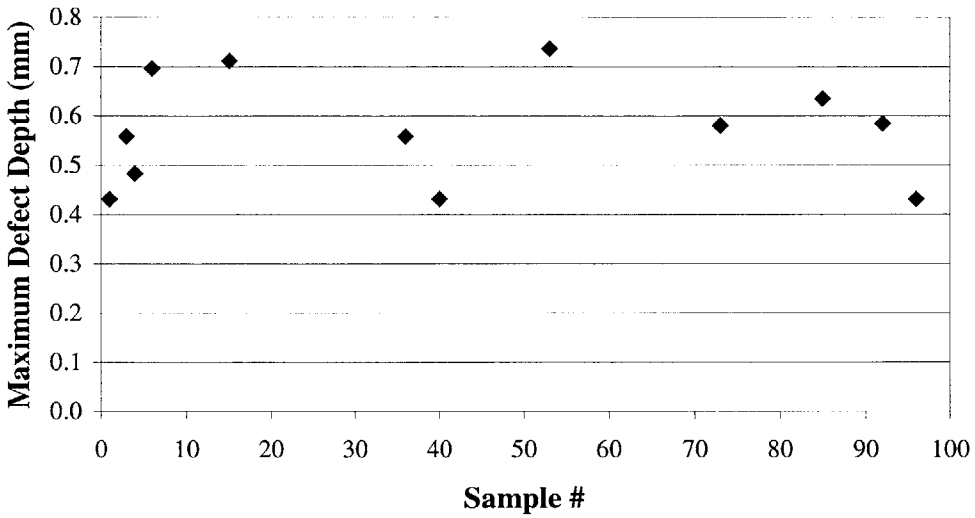

Figure 4.4. *Maximum defect depth versus location for 9-add whole shell test.*

As the analysis of DOE4 suggested, the product is not uniform along the shell length. There was a clear DVAL in the size of the diametrical dimensions, spanning from 20-40% of the defined tolerance ranges. This was not the case for width dimensions, however, which spanned less than 8% of their defined tolerance ranges. The TIR increased by a noticeable amount in the 9-add radial dimensions, but not in any dimensions of the 7-add part. The severity of surface defects appeared to be independent of shell location. The only significant variation along the shell length appears to occur in the product diameters.

4.2. PRM Main Drive Current Profile

Unfortunately, there is no simple and accurate process to directly monitor variation in the gorge or the roll force during the forming process at Tryon Peak. Fortunately, Equation 3.11 relates the main drive current to the roll force, and Equation 3.12 relates the roll force to the gorge. Therefore, an increase in the main drive current would represent an increase in the roll force, and also the gorge. By applying Equation 3.8, an increase in the roll force would also suggest an increase in the material flow stress. Since the DVAL was shown to be a linear function, the main drive current should also increase linearly.

By using a standard current sensor, the continuous amperage profile for the main drive current can be gathered for an entire shell. After gathering the amperage profile for four random non-sequential 9-add shells all produced at the same PRM conditions, a linear trendline was fit to the data, as shown in Figure 4.5. (See Appendix C for complete data.)

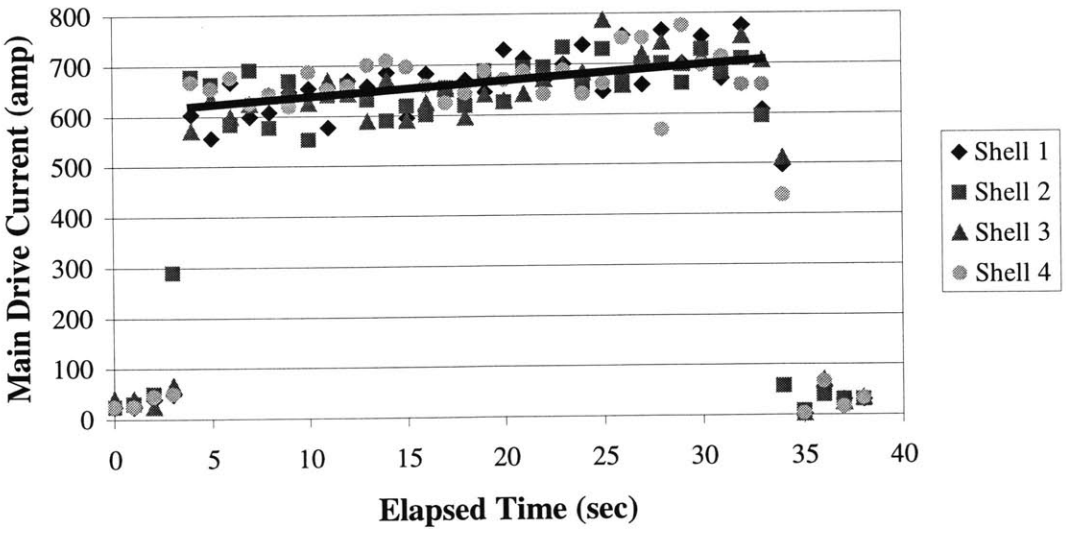

Figure 4.5. *Four 9-add amperage profiles.*

The main drive current is proportionally low before and after the forming process, because the forming rolls are still turning and requiring power, but they are not exerting any force to form a shell. Once the forming process begins, the main drive current immediately increases significantly. As expected, in all four shells sampled, the main drive current consistently increased linearly by approximately 100 amperes throughout the entire forming process, or 17% of the initial 600 amps provided at the beginning of the forming process. Three important conclusions may be drawn from the existence of this gradient. By applying Equation 3.11, a 17% increase in the main drive current gradient requires a similar significant increase in the roll force. (Although the Tryon Peak facility is currently unable to verify this roll force profile, the Research facility does have this capability. See Appendix F for Research data that illustrates an increase in the roll force during the forming process.) An increase in the roll force causes an increase in the gorge, as expressed by Equation 3.12, but it also suggests an increase in the material flow stress, as expressed by Equation 3.8. Further improvements should allow for the forming roll force and the gorge to be continuously monitored directly.

4.3. Temperature Profile

The standard process for measuring the temperature of hot steel in production is to use an optical pyrometer. For the PRM however, it is very difficult to collect accurate continuous temperature data at the exact time of forming because of smoke produced during the process and the inaccessibility to the material within the machinery. Therefore, it is necessary to develop a model to approximate the forming temperature, as explained in Section 3.1. Once the forming temperature is known, it can be directly related to the flow stress by Equations 3.2 and 3.3, and ultimately to the final product size by Equation 3.14 and the DVAL by Equation 3.15.

4.3.1. Shell Temperature Profile

The STP model predicts that the rear of the shell is hotter than the front of the shell at any given point in time, because of the previous operations performed, as explained in Section 3.1.2. Since the standard optical pyrometer is only capable of determining the shell temperature at one specific location at one specific point in time, it is not capable of determining a temperature profile along the length at one given instant in time. Therefore, it was necessary to use an advanced optical camera, which is capable of taking a picture of the entire shell, not just one location, at one instant. Using techniques similar to those of a standard optical pyrometer, the varying colors along the shell length can be translated into a temperature profile. Using this technique, the rear of the billet and subsequent shell was determined to be hotter than the front by 15-20°C and 25-40°C, respectively.[2]

As expected, the front of the shell is cooler than the back of the shell, and the difference is larger for the pierced shell. While this identifies a temperature gradient in the shell, it does not necessarily represent the variation in the entry temperature. The STP model assumes that this profile remains constant throughout the forming process, and is thus representative of the entry temperature and forming temperature profiles. Therefore, Equations 3.14 and 3.15 would predict that the decrease in the forming temperature would result in a decrease in the size of the final product, which contradicts the results of the whole shell tests. Therefore, either the initial assumption that the entry temperature profile is representative of the forming temperature profile is incorrect, or the shell temperature profile and the entry temperature profile are different.

4.3.2. Entry Temperature Profile

The ETP model attempts to expand upon the STP model to include radiant cooling of the rear of the shell during the lengthy forming process. From our continuous current profile, the complete forming time for a 9-add shell can be determined to be 30 seconds. Therefore, the rear half of the shell remains exposed to the air for approximately 15 seconds before entering the mill. As a result, Equation 3.1 predicts that the entry temperature will decrease by approximately 80°C for the rear half of the shell. Therefore, although the shell temperature profile was established to be approximately 20°C for the rear half of the shell, the 80°C decrease at the rear of the shell will result in the actual entry temperature decreasing by approximately 60°C for the rear half of the shell. This entry temperature profile predicted by the ETP model is significantly different from the 20°C increase predicted by the STP model.

By repositioning the standard optical pyrometer on the entry table and reprogramming the attached data logger, the continuous entry temperature profile can be measured for an entire shell, as shown in Figure 4.6.

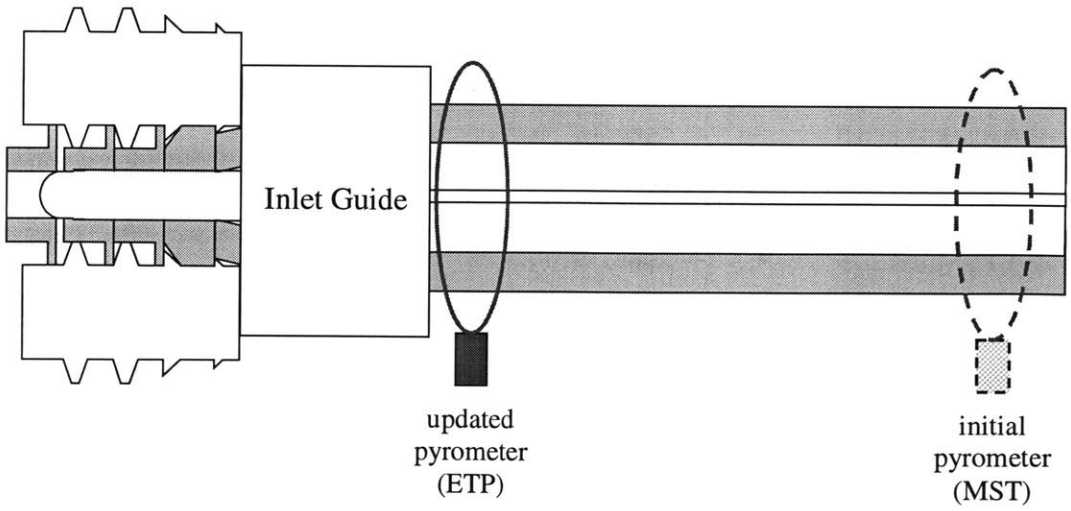

Figure 4.6. *Schematic setup for recording continuous entry temperature profile.*

When the shell first enters the mill, approximately the first half passes rapidly past the pyrometer until the front of the shell reaches the beginning of the forming rolls and the forming process begins. Therefore, continuous data is only available for the rear half of the shell. After collecting the entry temperature profiles for five shells intermittently, a linear trendline was fit to the data, as shown in Figure 4.7. (See Appendix D for complete data.) It is clear from this figure that the entry temperature for the rear half of the shell decreased uniformly by 70°C.

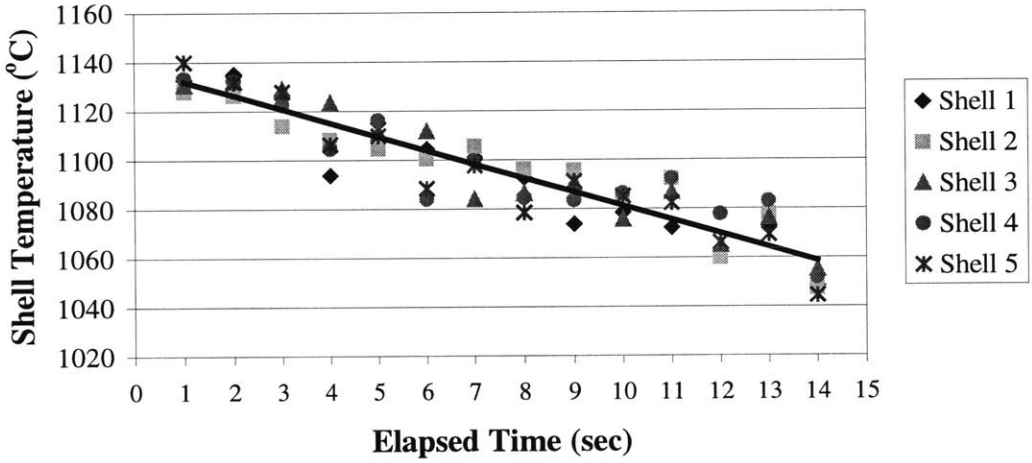

Figure 4.7. *Five 9-add entry temperature profiles.*

4.3.3. Summary of Temperature Testing

The STP model accurately predicts the profile of the shell prior to forming, but this profile is not representative of the actual entry temperature profile determined. The actual entry temperature profile shows that the rear of the shell is 70°C cooler than the middle of the shell at the time of entry into the mill. This is significantly different from the 20°C increase proposed by the STP model. The large fans that blow across the PRM in order to remove as much smoke as possible from the area are the primary source of the difference between the actual gradient and

the 60°C gradient predicted by the ETP model. This additional cooling effect was not taken into account in the simple model that was used to derive Equation 3.1. Regardless, it is clear that at the point of entry into the Profile Ring Mill, the material temperature is decreasing significantly over time. Equation 4.2 predicts that the entry temperature profile measured would cause the material flow stress to increase significantly by up to 23% for the rear half of the shell.

4.4. Maximum Shell Temperature versus Final Product Size

While the ETP model relates the variations in the entry temperature and the main drive current to the final product size, it would be ideal to investigate directly the relationship between the forming temperature and final size of each preform. Although this is not currently feasible, there is a significant amount of production data available that includes both the final product size and the maximum shell temperature. While, the MST method cannot be used to predict the variation in the forming temperature, Equation 3.14 predicts that for multiple shells formed at the same machine settings, an increase in the shell temperature would result in a decrease in the size of the final product.

Although, the maximum shell temperature has been recorded for every shell, air-cooled samples are only collected from every 6^{th} shell. Also, adjustments are frequently made to various operating parameters during production in order to optimize the quality of the final product. Therefore, it is difficult to find sufficient data points at the same parameters for analysis. Fortunately, quenched samples are gathered twice as often from every 3^{rd} shell. Since there is a known direct offset in size between the quenched and air-cooled preforms, the quenched samples can be used to represent the final product. It is important to note that only one quenched sample is gathered for each shell, and its exact location within that shell will vary from shell to shell.

During a 9-add production run, there were 29 quenched samples collected for shells produced at the exact same settings. For each sample collected, the corresponding maximum shell temperature was also recorded. After plotting the size of the SROD and LROD versus the maximum shell temperature, a trendline was fit to each set of data, as shown in Figure 4.8. (See Appendix E for complete run data.)

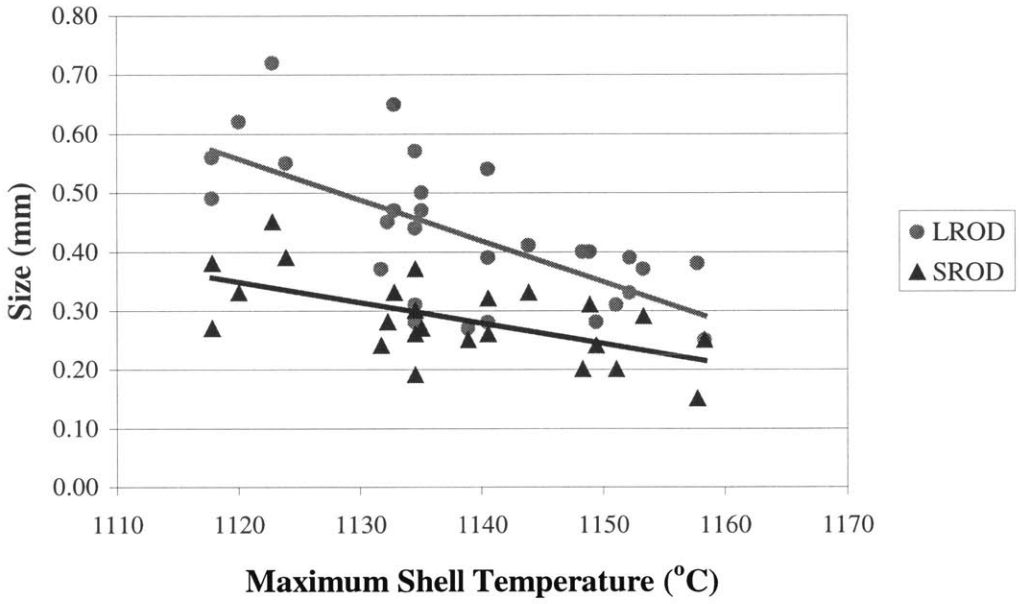

Figure 4.8. *Maximum shell temperature versus final product size for 9-add production.*

Although the maximum shell temperature is not an exact representation of the forming temperature and quenched samples are not an exact representation of the final product, they are sufficient for comparing the general characteristics of one shell to another shell. It is clearly shown in Figure 4.8 that as the magnitude of the shell temperature increases, the size of the product decreases. Over a 45°C increase in the maximum shell temperature, the LROD size decreased by 0.25 mm and the SROD size decreased by 0.15 mm. This is the exact relationship that the ETP model predicted.

Chapter 5: Conclusions and Recommendations

5.1. Conclusions

An extended analysis of the design of experiments identified the existence of non-uniformity in the preforms produced from the same shell in the PRM. The collection and analysis of an entire shell of preforms confirmed the DVAL by determining that the product diameters increased by 0.2-0.4 mm or 20-40% of the specified tolerance. Further investigations show that the ETP model accurately predicts the existence of a gradient in the entry temperature and the main drive current for the PRM. By applying the relationships derived in Section 3, the existence of these two gradients predict that the forming temperature decreases by up to 70°C and the material flow stress increases by up to 23% over the rear half of the shell, and the roll force increases by up to 17% over the entire shell. As a result, the gorge will swell, springback will increase, shrinkage will decrease, and the final product diameter will be larger. Analysis of 9-add production data also illustrates that as the overall shell temperature decreases, the overall product diameter increases.

There are further tests that can be conducted to provide additional support for the ETP model. For example, the roll force profile has not yet been collected on the production equipment. This can be achieved by reprogramming the data collection system. Also, the actual forming temperature has not yet been measured, at either facility. While there have not been any ideas to date that would enable these measurements, future efforts to address this need could be considered. The entry temperature has been used to predict the forming temperature by disregarding adiabatic heating. While a theoretical model could be developed to predict this heating effect, measuring the exit temperature would also be of great assistance in understanding

what happens inside the PRM. Also, the effects of the temperature gradient have been illustrated, but the relative importance of the individual process phenomenon remains to be investigated.

While these additional sources of data may provide additional information, corrective actions can be taken without them. The proposed ETP model relating the effects of temperature to preform diameter size has already been clearly verified. It has been shown that the shell temperature is decreasing significantly during the forming process and as a result the preforms produced from the rear of the shell are larger than the preforms from the front of the shell. It is also clear that in order to prevent significant DVAL, which can potentially result in increased scrap, the material temperature throughout the entire forming process, as well as from shell to shell, must be controlled.

Now that the significant temperature variation has been established as the root cause of the DVAL, it is necessary to develop system improvements to reduce, or ideally prevent, this problem. There are several different possible approaches to addressing this problem. One approach is to reduce the effects of temperature variation by redesigning the PRM process, or the PRM equipment itself. The other approach is to control the material temperature in order to maintain a constant forming temperature, throughout both an entire shell and from shell to shell. Temperature control could be achieved by minimizing the cooling time, maintaining a constant temperature, or controlling the rates of cooling.

5.2. PRM Equipment Changes

The possibility of adapting the PRM to be more robust and "immune" to temperature variation would be an ideal solution. Unfortunately, there are not any immediate changes that can be made to achieve this effect completely. Increasing the pressure on the hydraulic locks can

reduce the gorge swelling, but since the variations in springback and shrinkage are still temperature dependent, they cannot be resolved by simply changing the PRM design. Therefore other solutions must be considered.

5.3. Temperature Control System

Since equipment design changes will be insufficient, the only option is to reduce the amount of temperature variation. The first option is to decrease the total forming time per shell. This can be achieved by either adjusting the PRM settings or decreasing the shell length. Increasing the roll speed and the feed angle will increase the throughput time slightly, but there are also quality issues that arise with these adjustments. Reducing the shell size will also increase the throughput time, but it will ultimately reduce the rate of production, because the throughput time per piece will be lower. Therefore, the downsides of implementing these changes to reduce the cooling time far outweigh the slight benefits possibly gained.

Another option is to maintain a constant shell temperature. In order to keep the material temperature constant above 1800°F, it is necessary to install an in-line heating element. By installing an in-line heating element, the exact temperature of the shell can be controlled. While this improvement would be ideal, there are still a few problems. It will be difficult to install an in-line heating element at the PRM entry that is capable of heating the shells without heating the surrounding equipment. Although it is feasible, the cost of installation and maintenance is likely to be high. It may also introduce a potential safety hazard or hamper the operator's ability to monitor the process. Therefore, although an in-line heating element is feasible and might be ideal for maintaining a constant shell temperature, it is likely to be too expensive and may also introduce other negative results.

The last option is to control the cooling rates of the shell. It is clear that the 40°C variation initially present is not sufficient to produce a constant forming temperature. Therefore, either the rate of cooling must be reduced during forming, or the gradient prior to forming must be increased. One simple way to reduce the rate of cooling at the rear of the shell during forming is to turn off the large fans blowing across the entry table. These fans were not accounted for in the ETP profile, but they were the primary reason why the ETP underestimated the rate of cooling. If the fans are positioned elsewhere, they should still be able to blow a large portion of the smoke out of the way without cooling the shell. There are other options to reduce the radiant cooling at the entry table, such as installing an in-line heating element or enclosing the entry table. Whether or not an in-line heating element or an enclosure is sufficient, it will not be easy to install either device because of the PRM design.

Increasing the gradient in the shell prior to the PRM can be achieved in two different ways: decrease the temperature at the front of the shell, or increase the temperature at the rear of the shell. Properly positioned fans along the transfer route to the PRM could be used to accelerate the rate of cooling across the front of the shell. The rate of cooling at the rear of the shell could be reduced by either installing an in-line heating element, or simply enclosing a portion of the distance traveled with an insulated or reflective material. Both of these options should be inexpensive and can be implemented immediately.

5.4. Process Improvements

There is also a process change that could be introduced to reduce the effects of temperature variation. Currently, the shell temperature is only recorded, but it is not integrated into the actual forming process. Since it has been shown that the magnitude of the temperature of the shell is equally as important as the temperature variation, only shells within a specified

temperature tolerance or profile should be formed. A second optical pyrometer could be installed, if necessary, to estimate the temperature profile. Shells that are too hot, should simply be held on the entry table until their temperature has reduced to the acceptable tolerance, and then be entered into the PRM. Although unacceptable shells cannot be reworked, it is disadvantageous to form them. Not only is tool life wasted producing bad parts, but also unless there is a system in place to remove these pieces from the standard flow, they will produce a quality problem downstream. The only drawback to not forming the bad shell is that the cooling conveyor requires hot preforms to maintain a high ambient temperature and reduce the rate of cooling after forming. It is not clear at this time whether or not one set of preforms would significantly affect this process.

5.5. Final Recommendations

There are several possible solutions that could be implemented to ensure a more desirable temperature profile and thus reduce the DVAL. Redesigning the PRM to be more tolerant of temperature variation is not a feasible option. Incorporating an in-line heating system might be ideal, but it would be difficult and expensive to install. A simpler alternative would be to enclose the rear of the shell for a portion of the transfer route. A more detailed improvement would be to utilize the shell temperature sensors at the PRM entry data to validate that the shell temperature, or possible profile, is within a specified tolerance.

The importance of reducing the DVAL should not be downplayed. DVAL exists for every part currently produced, and for every potential part. The existence of significant DVAL will continue to result in increased, and unacceptable, levels of scrap. Whatever possible solution is implemented, it is crucial to control the material temperature throughout the entire forming process in order to ensure the production of uniform product.

Appendix A: Design of Experiments Data

There were eighteen different shells formed during the fourth Design of Experiments (DOE4). The feed angle was varied between 215', 230', and 245'. The lead was varied between 6 mm, 19 mm, and 32 mm. All of the settings known to affect the billet temperature or shell dimensions were constant, but there was still some small variation in these parameters. The same settings for tests 1-9 were duplicated in tests 10-18, as shown in Table A.1. A front (F), middle (M), and rear (R) sample was collected from each of the eighteen shells. All samples were both gauged and microanalyzed, as shown in Tables A.2a and A.2b.

Table A.1. *DOE4 test settings and operating parameters.*

Run #	Sample #	Billet Temperature	Forming Mill Settings			Shell Dimensions		
			Maximum Main Drive Current	Feed Angle	Lead	OD	ID	Wall
		F	amps	min	Mm	Mm	Mm	mm
1	126	2114	806	230	32	101.21	71.89	14.66
2	132	2129	793	215	6	101.20	71.88	14.66
3	138	2123	762	215	19	101.08	71.72	14.68
4	144	2109	857	230	6	101.17	71.99	14.59
5	150	2116	813	230	19	101.23	72.05	14.59
6	156	2128	857	245	32	101.20	71.90	14.65
7	162	2150	870	245	19	101.18	72.04	14.57
8	168	2127	775	215	32	101.18	71.88	14.65
9	174	2144	934	245	6	100.98	71.76	14.61
10	72	2127	806	230	32	101.17	71.99	14.59
11	78	2147	764	215	6	101.11	71.85	14.63
12	84	2151	742	215	19	101.09	71.87	14.61
13	90	2150	802	230	6	101.05	71.83	14.61
14	96	2151	826	230	19	101.12	72.06	14.53
15	102	2170	872	245	32	101.05	71.81	14.62
16	108	2176	839	245	19	101.06	71.82	14.62
17	114	2161	755	215	32	101.08	72.06	14.51
18	120	2162	837	245	6	101.09	71.87	14.61

Table A.2a. *Gauging and microanalysis data. (Shells 1-9)*

Run #	Sample #	Small Rib OD		Large Rib OD		Overall Width		Rib Width		Wall	Large Rib ID		Small Rib ID		Max. Lap Depth
		TIR	Size	TIR	Size	TIR	Size	TIR	Size	TIR	TIR	Size	TIR	Size	
		mm	mm	mm	mm	mm	mm	mm	mm	mm	mm	mm	mm	mm	mm
1	126F	0.10	-0.30	0.17	-0.05	0.14	-0.17	0.09	0.13	0.23	0.10	0.39	0.15	-0.17	0.316
1	126M	0.11	-0.21	0.05	-0.10	0.16	-0.09	0.13	0.17	0.48	0.13	0.49	0.32	-0.09	0.298
1	126R	0.08	-0.14	0.09	0.04	0.15	-0.03	0.14	0.16	0.46	0.40	0.54	0.44	0.04	0.316
2	132F	0.12	-0.34	0.20	-0.28	0.23	-0.38	0.19	-0.01	0.30	0.20	-0.52	0.22	-0.39	0.526
2	132M	0.11	-0.31	0.13	-0.23	0.08	-0.12	0.08	0.16	0.60	0.13	-0.26	0.16	-0.29	0.579
2	132R	0.09	-0.22	0.08	-0.14	0.12	-0.02	0.14	0.20	0.33	0.21	-0.11	0.31	-0.06	0.421
3	138F	0.08	-0.52	0.12	-0.24	0.15	-0.44	0.18	-0.04	0.25	0.21	-0.05	0.09	-0.12	0.228
3	138M	0.11	-0.44	0.17	-0.25	0.21	-0.20	0.21	0.12	0.30	0.31	0.11	0.28	0.13	0.526
3	138R	0.08	-0.30	0.06	-0.14	0.15	-0.09	0.15	0.20	0.19	0.26	0.25	0.17	0.14	0.281
4	144F	0.04	-0.17	0.16	-0.14	0.22	-0.19	0.22	0.09	0.31	0.27	-0.50	0.08	-0.44	0.491
4	144M	0.06	0.01	0.05	-0.06	0.12	0.03	0.10	0.23	0.49	0.14	-0.24	0.22	-0.22	0.509
4	144R	0.03	0.01	0.04	-0.02	0.08	0.03	0.04	0.21	0.25	0.11	-0.19	0.23	-0.14	0.404
5	150F	0.18	-0.36	0.17	-0.15	0.32	-0.34	0.36	0.05	0.69	0.19	-0.21	0.12	-0.18	0.281
5	150M	0.05	-0.25	0.03	-0.11	0.21	-0.18	0.54	0.04	0.30	0.13	-0.12	0.10	-0.07	0.351
5	150R	0.16	-0.10	0.23	-0.06	0.24	0.02	0.68	-0.09	0.90	0.18	-0.05	0.11	0.09	0.351
6	156F	0.16	-0.12	0.32	-0.22	0.15	-0.15	0.17	0.15	0.22	0.23	-0.21	0.22	-0.31	0.491
6	156M	0.17	-0.06	0.07	-0.21	0.14	-0.05	0.10	0.19	0.16	0.36	-0.15	0.34	-0.24	0.614
6	156R	0.11	0.00	0.11	-0.11	0.09	-0.03	0.11	0.20	0.26	0.31	-0.18	0.12	-0.25	0.702
7	162F	0.15	-0.25	0.21	-0.08	0.13	-0.23	0.26	0.15	0.43	0.18	-0.25	0.31	-0.17	0.368
7	162M	0.09	-0.05	0.13	-0.07	0.23	-0.08	0.32	0.23	0.28	0.10	-0.24	0.10	0.01	0.368
7	162R	0.18	0.06	0.11	-0.05	0.18	-0.01	0.16	0.24	0.54	0.22	-0.06	0.28	0.11	0.491
8	168F	0.30	-0.54	0.47	-0.37	0.48	-0.29	0.39	0.07	0.33	0.36	0.40	0.40	-0.14	0.351
8	168M	0.17	-0.51	0.26	-0.31	0.24	-0.13	0.18	0.16	0.26	0.21	0.68	0.23	0.00	0.351
8	168R	0.08	-0.35	0.14	-0.22	0.12	-0.04	0.12	0.22	0.60	0.26	0.70	0.12	0.05	0.386
9	174F	0.10	-0.28	0.18	-0.06	0.21	-0.42	0.23	-0.06	0.18	0.09	-0.63	0.15	-0.39	0.386
9	174M	0.03	0.13	0.12	-0.11	0.14	0.05	0.14	0.23	0.39	0.28	-0.31	0.25	-0.08	0.737
9	174R	0.18	0.14	0.15	-0.03	0.18	0.06	0.19	0.26	0.31	0.29	-0.07	0.34	-0.02	0.561

Table A.2b. *Gauging and microanalysis data. (Shells 10-18)*

Run #	Sample #	Small Rib OD		Large Rib OD		Overall Width		Rib Width		Wall	Large Rib ID		Small Rib ID		Max. Lap Depth
		TIR	Size	TIR	Size	TIR	Size	TIR	Size	TIR	TIR	Size	TIR	Size	
		mm	mm	mm	mm	mm	mm	mm	mm	mm	mm	mm	mm	mm	mm
10	**72F**	0.11	-0.41	0.26	-0.23	0.22	-0.23	0.13	0.12	0.24	0.28	0.29	0.33	-0.21	0.351
10	**72M**	0.17	-0.34	0.27	-0.29	0.34	-0.13	0.19	0.14	0.34	0.33	0.19	0.34	-0.08	0.404
10	**72R**	0.27	-0.07	0.18	-0.18	0.27	-0.03	0.35	0.25	0.71	0.31	0.37	0.26	0.17	0.351
11	**78F**	0.16	-0.51	0.36	-0.46	0.39	-0.49	0.45	-0.10	0.15	0.32	-0.53	0.31	-0.29	0.439
11	**78M**	0.04	-0.45	0.30	-0.41	0.80	0.00	0.51	-0.02	0.93	0.31	-0.27	0.30	-0.15	0.263
11	**78R**	0.06	-0.41	0.11	-0.35	0.10	-0.14	0.14	0.13	0.98	0.17	-0.23	0.31	-0.07	0.351
12	**84F**	0.14	-0.51	0.11	-0.34	0.17	-0.47	0.22	-0.05	0.27	0.26	-0.14	0.31	-0.08	0.263
12	**84M**	0.14	-0.50	0.33	-0.32	0.45	-0.32	0.19	0.15	0.51	0.39	0.03	0.19	0.14	0.333
12	**84R**	0.06	-0.42	0.16	-0.29	0.21	-0.15	0.17	0.19	0.34	0.24	0.19	0.27	0.25	0.316
13	**90F**	0.10	-0.40	0.08	-0.34	0.12	-0.23	0.09	0.11	0.63	0.61	-0.66	0.27	-0.29	0.386
13	**90M**	0.13	-0.29	0.17	-0.24	0.23	-0.15	0.19	0.17	0.48	0.33	-0.23	0.26	-0.08	0.386
13	**90R**	0.20	-0.12	0.15	-0.19	0.14	-0.02	0.19	0.23	0.71	0.32	-0.09	0.27	0.12	0.246
14	**96F**	0.12	-0.43	0.24	-0.23	0.26	-0.34	0.16	0.05	0.28	0.23	-0.31	0.29	-0.27	0.228
14	**96M**	0.08	-0.35	0.07	-0.30	0.12	-0.11	0.13	0.16	0.28	0.09	-0.14	0.21	-0.05	0.333
14	**96R**	0.28	-0.27	0.07	-0.26	0.23	-0.06	0.17	0.21	0.45	0.34	-0.06	0.44	0.04	0.474
15	**102F**	0.18	-0.26	0.10	-0.22	0.29	-0.25	0.25	0.11	0.73	0.21	-0.15	0.33	-0.31	0.404
15	**102M**	0.28	-0.03	0.12	-0.25	0.14	-0.02	0.32	0.23	0.81	0.22	-0.07	0.33	-0.03	0.404
15	**102R**	0.17	0.04	0.22	-0.23	0.10	0.01	0.13	0.25	0.34	0.29	-0.03	0.36	0.02	0.456
16	**108F**	0.12	-0.21	0.07	-0.25	0.24	-0.14	0.26	0.21	0.62	0.20	-0.38	0.18	-0.16	0.509
16	**108M**	0.10	-0.13	0.11	-0.29	0.05	-0.07	0.09	0.24	0.38	0.18	-0.29	0.15	-0.11	0.474
16	**108R**	0.05	0.00	0.27	-0.24	0.18	-0.04	0.14	0.22	0.25	0.27	-0.17	0.12	0.07	0.526
17	**114F**	0.08	-0.70	0.18	-0.54	0.16	-0.29	0.18	0.11	0.23	0.34	0.31	0.34	-0.24	0.316
17	**114M**	0.18	-0.62	0.26	-0.44	0.34	-0.20	0.32	0.11	0.41	0.23	0.60	0.29	0.00	0.263
17	**114R**	0.10	-0.32	0.15	-0.28	0.24	-0.04	0.15	0.20	0.39	0.41	0.72	0.43	0.17	0.316
18	**120F**	0.08	-0.38	0.13	-0.20	0.07	-0.55	0.15	-0.06	0.25	0.12	-0.63	0.18	-0.37	0.684
18	**120M**	0.08	-0.13	0.07	-0.27	0.11	-0.03	0.08	0.21	0.39	0.29	-0.24	0.25	-0.08	0.509
18	**120R**	0.09	0.05	0.05	-0.16	0.15	0.02	0.08	0.24	0.39	0.28	-0.04	0.33	0.03	0.667

Appendix B: Whole Shell Test Data

The gauging and microanalysis data from the entire 9-add shell of product collected is shown in Tables B.1a, B.1b and B.1c. The samples were collected in order, with sample 1 at the front of the shell. Samples 23-28 were "caterpillared" together (denoted by a "*"), and were therefore excluded from the rest of the analysis. Since it was infeasible to microanalyze every sample, only 12 random samples were selected for microanalysis.

The gauging and microanalysis data from the entire 7-add shell of product collected is shown in Tables B.2a, B.2b, and B.2c. The samples were collected in order, with sample 1 at the front of the shell. Some preforms were damaged during the collection process and were not gauged (blank entries). No samples were microanalyzed for surface defects.

Table B.1a. *9-add whole shell data. (Samples 2-19)*

Sample	Small Rib OD		Large Rib OD		Overall Width		Rib Width		Wall	Large Rib ID		Small Rib ID		Max. Lap Depth
	TIR	Size	TIR	Size	TIR	Size	TIR	Size	TIR	TIR	Size	TIR	Size	
	mm	mm	mm	mm	mm	mm	mm	mm	mm	mm	Mm	mm	mm	mm
2	0.20	-0.48	0.12	-0.49	0.16	-0.03	0.32	0.43	0.39	0.28	0.65	0.39	-0.16	0.432
3	0.08	-0.07	0.06	-0.54	0.24	0.08	0.18	0.36	0.39	0.10	-0.44	0.10	-0.74	
4	0.15	-0.10	0.18	-0.46	0.16	0.04	0.18	0.37	0.29	0.28	-0.42	0.24	-0.65	0.559
5	0.30	0.00	0.17	-0.53	0.16	0.13	0.17	0.42	0.40	0.42	-0.45	0.44	-0.86	0.483
6	0.12	-0.01	0.17	-0.48	0.14	0.14	0.28	0.41	0.40	0.19	-0.36	0.23	-1.03	
7	0.38	0.01	0.29	-0.48	0.18	0.14	0.44	0.42	0.32	0.27	-0.33	0.49	-1.03	0.696
8	0.18	0.00	0.17	-0.45	0.15	0.16	0.31	0.49	0.90	0.51	-0.42	0.32	-1.05	
9	0.22	0.07	0.25	-0.46	0.20	0.12	0.30	0.45	0.32	0.24	-0.24	0.43	-1.05	
10	0.29	0.06	0.26	-0.44	0.18	0.16	0.41	0.45	0.81	0.13	-0.28	0.41	-1.07	
11	0.32	0.04	0.22	-0.43	0.20	0.14	0.46	0.42	0.26	0.10	-0.31	0.52	-1.07	
12	0.33	0.06	0.24	-0.44	0.19	0.15	0.45	0.44	0.56	0.30	-0.25	0.49	-1.04	
13	0.46	0.05	0.27	-0.42	0.20	0.15	0.38	0.40	0.63	0.25	-0.30	0.55	-1.08	
14	0.12	0.11	0.17	-0.40	0.19	0.13	0.38	0.43	0.32	0.26	-0.20	0.38	-1.07	
15	0.31	0.09	0.12	-0.44	0.23	0.16	0.50	0.44	0.41	0.22	-0.19	0.51	-1.10	
16	0.52	0.02	0.48	-0.51	0.26	0.14	0.50	0.44	0.70	0.60	-0.43	0.54	-0.99	0.711
17	0.36	0.03	0.38	-0.45	0.23	0.14	0.41	0.45	0.32	0.27	-0.30	0.45	-1.01	
18	0.41	0.02	0.26	-0.46	0.22	0.17	0.48	0.48	0.53	0.13	-0.28	0.44	-1.12	
19	0.23	0.07	0.32	-0.44	0.20	0.12	0.41	0.44	0.17	0.24	-0.32	0.27	-1.06	

Table B.1b. *9-add whole shell data. (Samples 20-60)*

Sample	Small Rib OD		Large Rib OD		Overall Width		Rib Width		Wall	Large Rib ID		Small Rib ID		Max. Lap Depth
	TIR	Size	TIR	Size	TIR	Size	TIR	Size	TIR	TIR	Size	TIR	Size	
	mm	mm	mm	mm	mm	mm	mm	mm	mm	mm	Mm	mm	mm	mm
20	0.22	0.00	0.24	-0.48	0.31	0.19	0.50	0.46	0.42	0.26	-0.08	0.39	-0.96	
21	0.25	-0.03	0.19	-0.51	0.12	0.11	0.24	0.47	0.39	0.37	-0.33	0.39	-1.00	
22	0.36	0.05	0.34	-0.44	0.24	0.18	0.50	0.45	0.29	0.33	-0.25	0.48	-1.10	
23*	0.24	0.00	0.25	-0.49	0.16	0.09	0.16	0.45	0.30	0.29	-0.49	0.38	-0.85	
24*	0.43	0.08	0.42	-0.41	0.11	0.16	0.41	0.48	0.45	0.41	-0.13	0.68	-1.23	
25*	0.36	0.10	0.35	-0.34	0.18	0.18	0.49	0.45	0.35	n/a	N/a	0.40	-1.25	
26*	0.32	0.13	0.43	-0.25	0.19	0.18	0.44	0.48	0.41	0.36	-0.02	0.34	-1.27	
27*	0.18	0.13	0.19	-0.38	0.13	0.15	0.41	0.43	0.28	0.32	-0.11	0.56	-1.31	
28*	0.09	0.08	0.18	-0.41	0.19	0.17	0.45	0.45	0.48	0.12	-0.10	0.30	-1.18	
29	0.12	0.07	0.30	-0.40	0.47	0.27	0.48	0.45	0.47	0.25	-0.12	0.38	-1.04	
30	0.44	0.08	0.19	-0.47	0.32	0.10	0.53	0.41	0.79	0.57	-0.30	0.52	-1.09	
31	0.20	0.04	0.10	-0.47	0.22	0.13	0.39	0.44	0.48	0.21	-0.16	0.30	-1.04	
32	0.59	0.05	0.54	-0.48	0.28	0.16	0.58	0.44	0.66	0.72	0.00	0.65	-0.96	
33	0.08	0.02	0.19	-0.48	0.20	0.15	0.31	0.41	0.57	0.68	-0.10	0.29	-0.84	
34	0.49	0.07	0.35	-0.45	0.24	0.16	0.44	0.45	0.64	0.38	-0.07	0.65	-0.92	
35	0.40	0.03	0.40	-0.50	0.28	0.14	0.65	0.38	0.56	0.40	0.08	0.57	-0.95	
36	0.21	0.06	0.21	-0.47	0.22	0.16	0.50	0.48	0.67	0.54	0.12	0.32	-0.92	
37	0.17	0.03	0.13	-0.48	0.18	0.17	0.51	0.48	0.50	0.35	-0.01	0.55	-0.85	0.559
38	0.31	0.08	0.18	-0.47	0.21	0.14	0.39	0.40	0.32	0.36	0.02	0.42	-0.94	
39	0.23	0.10	0.20	-0.44	0.23	0.16	0.40	0.47	0.74	0.69	-0.18	0.57	-0.89	
40	0.39	0.05	0.29	-0.45	0.22	0.14	0.56	0.46	0.44	0.29	0.02	0.63	-0.96	
41	0.49	0.10	0.29	-0.40	0.22	0.16	0.46	0.47	0.56	0.43	-0.04	0.70	-0.96	0.432
42	0.33	0.09	0.18	-0.46	0.21	0.16	0.48	0.48	0.88	0.56	0.04	0.41	-0.90	
43	0.33	0.07	0.22	-0.43	0.22	0.15	0.50	0.47	0.32	0.21	-0.07	0.59	-0.94	
44	0.51	0.05	0.35	-0.44	0.21	0.16	0.41	0.46	0.52	0.26	-0.07	0.59	-0.87	
45	0.50	0.08	0.25	-0.43	0.24	0.14	0.59	0.42	0.34	0.28	-0.01	0.72	-0.97	
46	0.55	0.08	0.37	-0.44	0.23	0.15	0.57	0.46	0.61	0.45	0.00	0.63	-0.88	
47	0.39	0.07	0.23	-0.43	0.24	0.17	0.53	0.47	0.28	0.38	-0.07	0.57	-0.97	
48	0.43	0.06	0.14	-0.38	0.27	0.17	0.47	0.46	0.56	0.46	0.14	0.60	-0.85	
49	0.42	0.11	0.26	-0.42	0.18	0.16	0.43	0.48	0.52	0.38	-0.03	0.58	-0.86	
50	0.30	0.12	0.12	-0.37	0.22	0.19	0.39	0.49	0.40	0.32	0.06	0.51	-0.88	
51	0.37	0.10	0.24	-0.40	0.17	0.17	0.38	0.46	0.54	0.24	-0.02	0.50	-0.84	
52	0.58	0.09	0.54	-0.40	0.25	0.15	0.55	0.46	0.52	0.61	-0.01	0.76	-0.82	
53	0.53	0.09	0.37	-0.40	0.18	0.18	0.37	0.46	0.23	0.62	0.16	0.60	-0.89	
54	0.55	0.10	0.42	-0.35	0.19	0.15	0.40	0.48	0.36	0.51	0.08	0.62	-0.85	0.737
55	0.45	0.10	0.28	-0.41	0.22	0.18	0.29	0.41	0.30	0.36	-0.06	0.54	-0.87	
56	0.51	0.11	0.39	-0.41	0.28	0.18	0.49	0.47	0.56	0.66	0.00	0.59	-0.83	
57	0.59	0.10	0.35	-0.41	0.17	0.17	0.48	0.42	0.23	0.69	-0.09	0.67	-0.92	
58	0.23	0.12	0.21	-0.31	0.20	0.19	0.42	0.47	0.73	0.23	0.06	0.37	-0.85	
59	0.47	0.08	0.38	-0.42	0.19	0.14	0.35	0.43	0.29	0.53	-0.10	0.57	-0.85	
60	0.47	0.08	0.46	-0.43	0.22	0.18	0.37	0.45	0.54	0.63	0.05	0.46	-0.78	

Table B.1c. *9-add whole shell data. (Samples 61-100)*

Sample	Small Rib OD		Large Rib OD		Overall Width		Rib Width		Wall	Large Rib ID		Small Rib ID		Max. Lap Depth
	TIR	Size	TIR	Size	TIR	Size	TIR	Size	TIR	TIR	Size	TIR	Size	
	mm	mm	mm	mm	mm	mm	mm	mm	mm	mm	Mm	mm	mm	mm
61	0.54	0.11	0.44	-0.44	0.20	0.14	0.66	0.32	0.50	0.54	-0.04	0.57	-0.85	
62	0.45	0.02	0.51	-0.45	0.22	0.17	0.49	0.49	0.66	0.75	0.14	0.55	-0.83	
63	0.46	0.09	0.42	-0.42	0.23	0.14	0.30	0.40	0.43	0.41	0.01	0.78	-0.75	
64	0.47	0.08	0.43	-0.44	0.17	0.15	0.37	0.43	0.78	0.60	0.09	0.50	-0.81	
65	0.69	0.06	0.78	-0.42	0.25	0.17	0.43	0.43	0.60	0.80	-0.05	0.92	-0.73	
66	0.56	0.11	0.63	-0.35	0.23	0.19	0.65	0.41	0.66	0.88	-0.01	0.48	-0.72	
67	0.41	0.14	0.31	-0.39	0.14	0.16	0.36	0.46	0.95	0.46	-0.01	0.53	-0.70	
68	0.42	0.18	0.49	-0.39	0.23	0.17	0.59	0.44	0.58	0.46	0.02	0.64	-0.85	
69	0.37	0.16	0.29	-0.31	0.21	0.17	0.40	0.50	0.73	0.35	0.01	0.59	-0.81	
70	0.67	0.18	0.71	-0.30	0.26	0.16	0.49	0.47	0.30	0.55	0.07	0.87	-0.83	
71	0.20	0.13	0.19	-0.29	0.26	0.20	0.48	0.50	0.80	0.49	0.20	0.56	-0.82	
72	0.41	0.19	0.30	-0.31	0.20	0.16	0.38	0.49	0.31	0.40	0.05	0.59	-0.72	
73	0.56	0.16	0.40	-0.29	0.22	0.18	0.48	0.44	0.24	0.50	0.07	0.66	-0.72	
74	0.32	0.21	0.24	-0.34	0.19	0.18	0.37	0.44	0.43	0.38	0.10	0.56	-0.75	0.580
75	0.55	0.16	0.48	-0.38	0.24	0.17	0.49	0.43	0.26	0.52	-0.02	0.71	-0.77	
76	0.24	0.24	0.32	-0.36	0.22	0.18	0.36	0.43	0.41	0.49	-0.10	0.58	-0.79	
77	0.33	0.13	0.19	-0.34	0.21	0.19	0.33	0.42	0.30	0.30	0.06	0.67	-0.81	
78	0.42	0.14	0.27	-0.39	0.21	0.19	0.48	0.43	0.32	0.42	0.03	0.50	-0.69	
79	0.51	0.08	0.33	-0.29	0.23	0.18	0.47	0.50	0.38	0.44	-0.01	0.62	-0.85	
80	0.49	0.09	0.41	-0.38	0.31	0.26	0.28	0.46	0.33	0.57	-0.02	0.43	-0.80	
81	0.49	0.23	0.28	-0.24	0.21	0.18	0.43	0.50	0.56	0.45	0.16	0.51	-0.91	
82	0.13	0.17	0.34	-0.28	0.19	0.20	0.43	0.42	0.56	0.32	-0.02	0.49	-0.86	
83	0.29	0.20	0.22	-0.30	0.18	0.17	0.37	0.48	0.58	0.34	0.22	0.31	-0.84	
84	0.36	0.15	0.31	-0.25	0.17	0.19	0.53	0.45	0.81	0.39	0.10	0.56	-0.84	
85	0.10	0.15	0.26	-0.26	0.30	0.23	0.47	0.50	0.37	0.29	0.15	0.25	-0.78	
86	0.36	0.12	0.32	-0.32	0.20	0.19	0.32	0.47	1.00	0.87	-0.39	0.47	-0.85	0.635
87	0.49	0.20	0.33	-0.30	0.23	0.16	0.48	0.37	0.41	0.68	0.11	0.64	-0.70	
88	0.47	0.11	0.29	-0.31	0.37	0.29	0.35	0.48	0.13	0.48	0.02	0.58	-0.69	
89	0.54	0.17	0.42	-0.33	0.20	0.19	0.33	0.45	0.47	0.37	-0.03	0.61	-0.74	
90	0.26	0.12	0.79	-0.11	0.29	0.20	0.50	0.48	0.44	0.36	0.09	0.26	-0.74	
91	0.62	0.04	0.53	-0.42	0.27	0.16	0.53	0.44	0.60	0.48	-0.02	0.74	-0.84	
92	0.46	0.20	0.25	-0.29	0.20	0.17	0.47	0.47	0.57	0.35	0.04	0.65	-0.69	
93	0.48	0.17	0.38	-0.33	0.23	0.19	0.39	0.42	0.46	0.57	0.10	0.58	-0.78	0.584
94	0.43	0.14	0.30	-0.35	0.16	0.20	0.39	0.45	0.48	0.33	0.16	0.56	-0.81	
95	0.58	0.17	0.48	-0.31	0.22	0.17	0.49	0.48	0.44	0.42	0.01	0.76	-0.73	
96	0.33	0.13	0.25	-0.33	0.26	0.18	0.41	0.45	0.44	0.31	0.02	0.64	-0.75	
97	0.34	0.14	0.21	-0.35	0.25	0.16	0.47	0.45	0.37	0.24	-0.01	0.54	-0.60	0.432
98	1.21	-0.17	1.21	-0.55	0.38	0.16	0.51	0.43	1.58	1.08	0.18	1.13	-0.49	
99	0.95	-0.13	0.95	-0.24	0.65	0.06	0.70	0.35	1.81	1.16	0.59	1.21	-0.13	
100	0.39	-0.38	0.45	-0.59	0.26	0.19	0.46	0.49	1.27	0.75	0.53	1.19	-0.30	

Table B.2a. *7-add whole shell data. (Shells 1-50)*

Sample #	Small Rib OD		Large Rib OD		Overall Width		Rib Width		Wall	Large Rib ID		Small Rib ID	
	TIR	Size	TIR	Size	TIR	Size	TIR	Size	TIR	TIR	Size	TIR	Size
	mm	mm	mm	mm	mm	mm	mm	mm	mm	mm	mm	mm	mm
1	0.11	0.28	0.11	0.06	0.11	-0.21	0.11	0.49	1.41	0.55	0.75		
3	0.41	0.12	0.29	0.00	0.47	-0.34	0.87	0.14	0.75	0.56	0.53	0.09	-0.21
4	0.16	0.16	0.15	0.05	0.24	-0.62	0.14	0.25	0.44	0.50	0.35	0.24	-0.31
5	0.32	-0.18	0.21	-0.04	0.40	-0.65	0.25	0.15	0.91	0.16	0.10	0.05	-0.72
6	0.74	0.20	0.76	-0.11					0.75	0.45	0.60	0.54	-0.04
7	0.18	-0.20			1.29	-0.47	0.79	0.21	1.09	0.42	0.24	0.16	-0.64
8	0.01	-0.21	0.10	-0.07	0.34	-0.83	0.59	-0.06	0.01	0.29	0.06	0.05	-0.49
9	0.13	-0.11	0.10	-0.02	1.17	-1.13	0.61	0.11	0.13	0.06	0.22	0.09	-0.78
10	0.09	-0.18	0.13	-0.04	0.18	-0.87	0.29	0.06	1.26	0.29	-0.12	0.17	-0.70
11	0.21	-0.09	0.24	-0.08	0.54	-0.80	0.24	0.27	1.53	0.15	0.19	0.22	-0.55
12	0.15	-0.12	0.20	-0.07	0.53	-0.65	0.47	0.24	0.42	0.44	0.45	0.23	-0.44
12	0.15	-0.01	0.09	-0.01	0.48	-0.64	0.32	0.23	0.67				
13	0.11	-0.07	0.18	-0.08	0.25	-0.70	0.63	-0.04	0.98	0.30	0.21	0.16	-0.57
14	0.15	0.04	0.17	0.02	0.11	-0.59	0.18	0.23	1.19	0.17	0.52	0.24	-0.27
15	0.08	-0.14	0.17	-0.07	0.39	-0.76	0.22	0.17	0.53	0.18	0.32	0.12	-0.50
17	0.16	-0.01	0.07	-0.01	0.20	-0.62	0.12	0.25	1.01	0.30	0.49	0.15	-0.43
19	0.18	0.28	0.16	0.11	0.15	-0.36	0.09	0.45	1.40	0.66	0.62	0.25	-0.38
20	0.17	-0.19	0.12	-0.08	0.36	-0.70	0.30	0.19	0.46				
22	0.12	-0.15	0.13	-0.08	0.33	-0.82	0.42	0.11	0.88	0.18	0.33	0.20	-0.48
23	0.19	-0.02	0.13	-0.06	0.54	-0.55	0.51	0.25	1.52	0.36	0.61		
24	0.14	-0.06	0.06	-0.10	0.26	-0.65	0.07	0.25	0.38	0.25	0.39	0.14	-0.36
25	0.18	-0.09	0.05	-0.06	0.45	-0.69			0.48	0.32	0.56	0.25	-0.48
27	0.12	0.00	0.09	-0.02	0.47	-0.56	0.24	0.18	0.62	0.16	0.52	0.21	-0.35
28	0.31	0.08	0.32	0.07	0.48	-0.49	0.10	0.21	0.97	0.36	0.49	0.41	-0.32
29	0.16	0.06	0.05	0.00	0.49	-0.58	0.58	0.22	0.60	0.53	0.61	0.42	-0.37
30	0.11	0.11	0.22	0.02	0.16	-0.45	0.13	0.37	0.29	0.46	0.70	0.17	-0.27
31	0.03	0.16	0.23	0.11	0.11	-0.46	0.15	0.38	0.81	0.26	0.56	0.28	-0.36
32	0.32	0.13	0.23	0.02			0.24	0.52	0.28	0.41	0.87	-0.56	-0.27
33	0.35	0.07	0.24	0.00	-0.58	-0.19	0.15	0.56	0.41				
35	0.15	0.14	0.11	0.02	-0.50	-0.20	-0.27	0.45	0.72	0.42	1.01	-0.40	-0.12
36	0.25	0.20	0.25	0.03	-0.51	-0.25	0.21	0.51	0.30	-0.01	0.46	-0.86	-0.48
37	0.22	0.27	0.32	0.03	-0.45	-0.15	0.33	0.54	0.22	0.05	0.84	-0.46	-0.10
38	0.27	0.24	0.20	0.03	-0.38	-0.14	0.03	0.55	0.52	0.50	0.92	-0.33	-0.05
39	0.40	0.36	0.44	0.12	-0.34	-0.17	0.39	0.53	0.14			-0.83	-0.25
40	0.09	0.33	0.14	0.05	-0.29	-0.16	0.35	0.51	0.17	0.52	0.93	-0.22	0.04
42	0.23	0.32	0.22	0.09	-0.32	-0.16	0.36	0.57	0.22	0.39	0.62	-0.64	-0.38
43	0.14	0.30	0.05	0.12	-0.28	-0.17	0.37	0.49	0.12	0.42	0.85	-0.40	-0.23
44	0.32	0.29	0.36	0.11	-0.32	-0.10	0.35	0.53	0.19	-0.06	0.85	-0.73	-0.53
45	0.21	0.40	0.26	0.10	-0.29	-0.09				0.37	1.06	-0.27	-0.09
46	0.38	0.34	0.47	0.08	-0.30	-0.17	0.34	0.54	0.20	0.48	1.08	-0.26	-0.01
48	0.19	0.33	0.12	0.00			0.35	0.53	0.18	0.32	0.89	-0.28	-0.23
50	0.19	0.31	0.10	0.04	-0.30	-0.12	0.39	0.54	0.15	-0.27	0.52	-0.68	-0.63

Table B.2b. *7-add whole shell data. (Shells 51-90)*

Sample #	Small Rib OD		Large Rib OD		Overall Width		Rib Width		Wall	Large Rib ID		Small Rib ID	
	TIR	Size	TIR	Size	TIR	Size	TIR	Size	TIR	TIR	Size	TIR	Size
	mm	mm	mm	mm	mm	mm	mm	mm	mm	mm	mm	mm	mm
51	0.09	0.24	0.15	0.01	-0.38	-0.15	0.42	0.50	0.08	-0.26	0.14	-0.90	-0.82
52	0.15	0.22	0.36	-0.01	-0.38	-0.26	0.27	0.53	0.26	0.30	1.30	-0.48	-0.13
53	0.31	0.31	0.10	0.06	-0.37	-0.16	0.26	0.47	0.21	0.35	0.60	-0.39	-0.08
54	0.03	0.27	0.06	0.11	-0.39	-0.21	0.25	0.49	0.24	0.53	1.01	-0.25	-0.10
55	0.05	0.30	0.10	0.08	-0.32	-0.24	0.43	0.52	0.08	0.65	1.04		
56	0.19	0.32	0.16	0.13	-0.39	-0.25	0.28	0.51	0.23	0.37	0.95	-0.17	0.00
57	0.22	0.27	0.19	0.12	-0.46	-0.23	0.07	0.45	0.38	0.22	0.69	-0.68	-0.39
58	0.14	0.27	0.23	0.08	-0.50	-0.19	0.01	0.45	0.44	0.34	1.15	-0.31	-0.07
59	0.12	0.32	0.19	0.12	-0.41	-0.12	0.37	0.44	0.07	0.51	0.85	-0.30	0.10
60	0.33	0.30	0.39	0.13	-0.34	-0.12	0.38	0.56	0.18	-0.21	0.53	-0.72	-0.44
62	0.14	0.31	0.20	0.14	-0.43	-0.22	0.44	0.53	0.10	0.43	0.97	-0.47	-0.13
63	0.23	0.33	0.18	0.08	-0.34	-0.29	0.28	0.44	0.16				
64	0.37	0.34	0.18	0.10	-0.31	-0.13	-0.17	0.52	0.69	0.74	1.10	-0.28	0.21
65	0.04	0.31	0.19	0.12	-0.33	-0.24	0.36	0.49	0.14	0.13	0.31	-0.46	-0.33
66	0.18	0.34	0.19	0.12			0.43	0.52	0.09	0.49	1.10	-0.51	-0.12
67	0.23	0.30	0.30	0.14	-0.48	-0.24	-0.22	0.44	0.66	0.63	1.14	-0.27	-0.04
68	0.29	0.22	0.34	0.15	-0.41	-0.19	0.26	0.47	0.21	0.51	1.19	-0.36	-0.06
69	0.25	0.29	0.26	0.11			0.37	0.56	0.19	0.13	0.81		
70	0.08	0.21	0.07	0.14	-0.52	-0.21	0.32	0.47	0.15	0.70	1.00	-0.23	-0.16
71	0.24	0.24	0.24	0.16	-0.45	-0.28	0.25	0.44	0.19	0.14	0.24	-0.78	-0.52
73	0.24	0.22	0.11	0.16	-0.52	-0.23	0.30	0.46	0.16	0.19	0.56	-0.65	-0.45
74	0.15	0.27	0.23	0.10	-0.45	-0.24	0.22	0.49	0.27	-0.05	0.80	-0.29	-0.20
75	0.21	0.29	0.10	0.25	-0.36	-0.23	0.47	0.51	0.03				
76	0.07	0.25	0.09	0.10	-0.44	-0.22	0.33	0.49	0.16	0.71	1.01	-0.22	-0.14
77	0.24	0.30	0.25	0.11	-0.44	-0.22	0.34	0.52	0.18			-0.27	0.06
78	0.08	0.28	0.07	0.10	-0.51	-0.46	0.35	0.46	0.11	0.43	1.04	-0.30	-0.15
79	0.10	0.27	0.10	0.15	-0.45	-0.19	0.38	0.44	0.05	0.59	0.77		
80	0.13	0.26	0.19	0.12	-0.48	-0.24	0.24	0.48	0.23	0.55	0.98	-0.24	-0.20
81	0.20	0.27	0.26	0.10	-0.36	-0.24	0.31	0.54	0.24	0.71	1.18	-0.20	-0.11
82	0.17	0.21	0.11	0.13	-0.51	-0.28	0.22	0.48	0.27	0.53	0.84	-0.34	-0.14
83	0.12	0.28	0.08	0.14	-0.51	-0.15	0.32	0.47	0.14	0.47	0.86	-0.25	-0.07
84	0.15	0.27	0.08	0.14	-0.49	-0.31	0.36	0.41	0.04	0.47	0.97	-0.22	-0.10
85	0.17	0.29	0.14	0.17	-0.43	-0.30	0.16	0.47	0.31	0.11	0.74	-0.56	-0.37
86	0.19	0.25	0.29	0.15	-0.56	-0.27	0.13	0.48	0.35	0.52	1.05	-0.31	0.03
87	0.25	0.19	0.18	0.19	-0.52	-0.22	0.28	0.45	0.18	0.48	0.99	-0.29	0.02
88	0.29	0.19	0.14	0.13	-0.49	-0.18	0.31	0.52	0.21	0.79	0.93	-0.37	-0.08
89	0.07	0.25	0.13	0.19	-0.49	-0.20	-0.06	0.45	0.51	0.58	0.88	-0.21	-0.09
90	0.15	0.25	0.20	0.11	-0.48	-0.31	0.34	0.41	0.08	0.43	1.02	-0.22	-0.12

Table B.2c. *7-add whole shell data. (Shells 91-124)*

Sample #	Small Rib OD		Large Rib OD		Overall Width		Rib Width		Wall	Large Rib ID		Small Rib ID	
	TIR	Size	TIR	Size	TIR	Size	TIR	Size	TIR	TIR	Size	TIR	Size
	mm	mm	mm	mm	mm	mm	mm	mm	mm	mm	mm	mm	mm
91	0.12	0.23	0.07	0.15	-0.50	-0.28	0.09	0.41	0.32	0.77	1.03	-0.28	-0.13
92	0.02	0.23	0.10	0.18	-0.51	-0.34	-0.01	0.40	0.41	-0.03	0.56	-0.81	-0.63
93	0.14	0.23	0.10	0.19	-0.47	-0.34	0.04	0.44	0.40	0.42	1.10	-0.26	-0.06
94	0.09	0.22	0.06	0.12	-0.47	-0.30	0.32	0.43	0.11	0.72	0.79	-0.22	-0.12
95	0.11	0.26	0.05	0.17	-0.51	-0.30	0.22	0.50	0.28			-0.31	-0.13
96	0.14	0.22	0.11	0.16	-0.58	-0.25	0.23	0.45	0.22	0.46	0.94	-0.26	-0.07
97	0.26	0.18	0.12	0.17	-0.56	-0.24	0.13	0.40	0.27	0.64	1.10	-0.31	-0.10
98	0.06	0.24	0.07	0.19	-0.49	-0.26	0.32	0.47	0.16				
99	0.17	0.26	0.03	0.19	-0.43	-0.19	0.19	0.42	0.22	0.40	1.01	-0.16	-0.04
100	0.23	0.31	0.24	0.15	-0.41	-0.37	0.33	0.48	0.14				
101	0.14	0.27	0.10	0.19	-0.46	-0.28				0.52	0.71	-0.07	-0.03
102	0.18	0.22	0.28	0.18	-0.57	-0.30	0.35	0.44	0.09				
103	0.15	0.27	0.14	0.17	-0.53	-0.33	0.21	0.47	0.26	0.49	1.07	-0.19	-0.13
105	0.09	0.22	0.11	0.19	-0.48	-0.36	0.33	0.52	0.19	0.58	1.03	-0.25	-0.09
106	0.11	0.24	0.10	0.17	-0.57	-0.26	0.28	0.54	0.26	0.23	0.86	-0.28	-0.14
107	0.12	0.26	0.28	0.17	-0.54	-0.26	0.23	0.46	0.23	0.26	1.02	-0.21	-0.06
109	0.19	0.08	0.41	0.07	-0.60	-0.18	0.17	0.51	0.34	0.33	0.42	-0.42	0.10
110	0.10	0.26	0.30	0.23	-0.37	-0.24	0.26	0.48	0.22	0.58	0.86	-0.29	-0.18
111	0.29	0.31	0.12	0.25	-0.59	-0.21	-0.48	0.47	0.95	0.74	1.02	-0.27	-0.19
112	0.21	0.33	0.13	0.26	-0.50	0.11	0.27	0.46	0.20	0.70	1.04	-0.21	0.07
113	0.11	0.26	0.15	0.22	-0.45	-0.27	0.27	0.49	0.22	0.46	0.58	-0.50	-0.41
114	0.07	0.22	0.17	0.22	-0.64	-0.32	-0.28	0.45	0.73	0.66	0.95	-0.26	-0.10
115	0.06	0.25	0.16	0.20	-0.57	-0.28	0.20	0.51	0.30	0.47	1.01	-0.40	-0.13
117	0.09	0.27	0.04	0.21	-0.42	-0.31	0.04	0.46	0.42	0.52	0.94	-0.20	-0.09
118	0.12	0.27	0.11	0.17	-0.41	-0.31	0.27	0.41	0.13	0.62	0.84	-0.30	-0.09
119	0.21	0.25	0.02	0.19	-0.52	-0.17	0.16	0.41	0.26	0.71	1.11	-0.19	-0.05
120	0.05	0.17	0.20	0.22	-0.65	-0.34	0.26	0.48	0.23	0.56	1.10	-0.28	-0.18
121	0.16	0.23	0.09	0.20	-0.52	-0.29	-0.56	0.43	0.99	-0.98	-0.48		
122	0.39	-0.02	0.35	-0.35	-0.23	0.03	0.37	0.45	0.09	-0.82	0.01	-1.20	-0.88
123	0.25	-0.13	0.35	-0.10	-0.46	0.06	0.04	0.45	0.40	0.53	1.12	-0.01	0.10
124	0.43	-0.13	0.40	-0.43	-0.27	-0.17	0.25	0.48	0.23	-0.40	0.57	-0.79	-0.17

Appendix C: PRM Main Drive Current Profile Data

The main drive current was continually monitored for four random intermittent 9-add shells. The data that was returned from the typical current sensor used was the average current that was supplied over the period of one second, as shown in Table C.1. Prior to forming, the main drive current is not zero because there is some electrical power required to keep the machine running, even if it is not forming.

Table C.1. *Continuous PRM main drive current for 4 non-sequential shells.*

Elapsed Time	Shell 1	Shell 2	Shell 3	Shell 4
sec	amp	amp	amp	amp
0	24	24	40	24
1	24	31	40	24
2	40	50	24	44
3	48	289	66	50
4	603	678	570	667
5	556	663	634	654
6	667	583	598	676
7	598	691	623	625
8	607	576	640	643
9	647	669	654	618
10	654	552	625	687
11	576	640	669	651
12	669	660	643	658
13	658	631	588	700
14	685	589	671	709
15	594	618	589	696
16	682	601	623	658
17	643	654	651	623
18	669	618	594	643
19	645	687	640	687
20	729	625	627	669
21	711	693	640	685
22	667	693	669	640
23	700	733	696	687
24	738	658	682	640
25	645	729	786	660
26	755	663	656	751
27	658	700	718	751
28	766	700	742	567
29	700	660	698	775
30	753	727	711	696
31	669	680	711	713
32	775	709	753	656
33	607	594	705	656
34	497	57	510	437
35	1	7	1	2
36	55	40	68	66
37	31	31	24	15
38	31	31	33	33

Appendix D: Entry Temperature Profile Data

The shell entry temperature was continually monitored for five random intermittent 9-add shells. The data that was returned from the typical optical pyrometer used was the average temperature over the period of one second, as shown in Table D.1. Since these temperature readings do not account for any scale that may have developed on the skin of the shell, these temperatures are minimum temperatures at the given point time. The actual shell temperature may be slightly higher. A visual inspection suggested that the scale appeared to be of the same magnitude and uniform along the length for all shells examined.

Table D.1. *Shell entry temperature profile data for five non-sequential 9-add shells.*

Elapsed Time	Shell 1	Shell 2	Shell 3	Shell 4	Shell 5
sec	°F	°F	°F	°F	°F
1	2071	2062	2067	2072	2084
2	2075	2059	2070	2070	2069
3	2060	2037	2064	2052	2062
4	2001	2027	2054	2020	2023
5	2039	2020	2032	2041	2030
6	2020	2012	2033	1983	1991
7	2014	2022	1983	2011	2008
8	1999	2005	1987	1984	1973
9	1965	2004	1995	1982	1996
10	1973	1986	1968	1987	1985
11	1962	1998	1988	1998	1980
12	1946	1940	1949	1972	1951
13	1963	1972	1969	1981	1957
14	1919	1917	1931	1925	1912

Appendix E: Maximum Shell Temperature v. Final Product Size Data

There is a vast amount of production data available for both the maximum shell temperature and the final product dimensions. The maximum shell temperature is recorded for every shell that is formed. Unfortunately, since product sampling is infrequent and changes to the production settings are frequent, there is minimal dimensional data available at the same production settings on the same tooling sets. Fortunately the dimensions of quenched samples can both be related to air-cooled samples and are collected twice as frequently. Therefore, the production run of 9-add parts from late September is sufficient for analysis. All of the data was gathered in accordance with the standard Tryon Peak operating procedures. The production settings are shown in Table E.1 and the partial dimensional analysis is shown in Table E.2.

Table E.1. *PRM production settings for 9-add part.*

Roll Speed	265 rpm
Feed Angle	329'
Lead	12.1 mm
Gorge	32.8 mm
Shell OD	104.6 +/- 0.1
Shell Wall	14.1 +/- 0.1

Table E.2. *Maximum shell temperatures and partial quenched product dimensions.*

Maximum Shell Temperature	Size of SROD	Size of LROD
2053	0.45	0.72
2048	0.33	0.62
2085	0.26	0.39
2101	0.24	0.28
2104	0.20	0.31
2108	0.29	0.37
2100	0.31	0.40
2116	0.15	0.38
2099	0.20	0.40
2071	0.33	0.65
2070	0.28	0.45
2071	0.33	0.47
2044	0.27	0.49
2075		0.50
2074	0.19	0.44
2044	0.38	0.56
2085	0.32	0.54
2091	0.33	0.41
2106		0.33
2106		0.39
2117	0.25	0.25
2074	0.30	0.28
2055	0.39	0.55
2074	0.37	0.57
2085		0.28
2069	0.24	0.37
2082	0.25	0.27
2074	0.26	0.31
2075	0.27	0.47

Appendix F: Roll Force Profile Data from Research

While the data collection system at Tryon Peak has not been programmed to continuously record the roll forces yet, the PRM test equipment installed at Research has this capability. Although, the mini-shells used at Research are only one-third of the length of the shells used at Tryon Peak, the roll speed has been reduced to ensure that the overall forming time is as similar as possible. Since, the mini-shells are shorter, they are not exposed to the open air outside of the mill for as long a duration as the regular shells. Using a standard pizeo-electric strain gage load cell, the average values over the period of one second are recorded each second to provide data continuously. The roll forces for all three rolls from the test run of the typical 3.0" 13-add part are shown in Table F.1. After plotting the roll forces and the PRM main drive current, a trendline was fit to the data, as shown in Figures F.1 and F.2, respectively. The trendlines do not include the near-zero data points that occur when there is no forming being performed.

Table F.1. *PRM main drive current and roll force data for 13-add part at Research.*

Elapsed Time	PRM Main Drive Current	Roll Force		
		Upper	Right	Left
sec	amps	N	N	N
0	33	5391.21	10806.59	9210.99
1	33	5367.03	10830.77	9210.99
2	33	5367.03	10806.59	9210.99
3	33	5415.38	10830.77	9210.99
4	65	5874.73	11217.58	9573.63
5	225	9186.81	13852.75	13514.29
6	530	16850.55	18736.26	21371.43
7	462	18083.52	21298.90	24828.57
8	555	18615.38	22580.22	25553.85
9	611	22362.64	25868.13	29035.16
10	582	22797.80	26230.77	29639.56
11	632	23039.56	26545.05	29978.02
12	640	23329.67	26762.64	30268.13
13	585	24828.57	27076.92	30413.19
14	681	24828.57	27149.45	30582.42
15	681	24997.80	27439.56	31114.29
16	681	26472.53	27898.90	31356.04
17	616	26665.93	28140.66	31597.80
18	703	26810.99	28213.19	31791.21
19	660	27415.38	28382.42	31984.62
20	660	27342.86	29010.99	32709.89
21	728	28068.13	29349.45	33024.18
22	477	19074.72	26303.30	26448.35
23	368	14892.31	23764.84	22362.64
24	338	13586.81	21685.71	19389.01
25	4	6672.53	14819.78	12740.66
26	13	5753.85	12643.96	10443.96
27	36	5705.49	12523.08	10516.48
28	36	5681.32	12474.73	10468.13
29	28	5632.97	12474.73	10492.31
30	28	5608.79	12474.73	10443.96

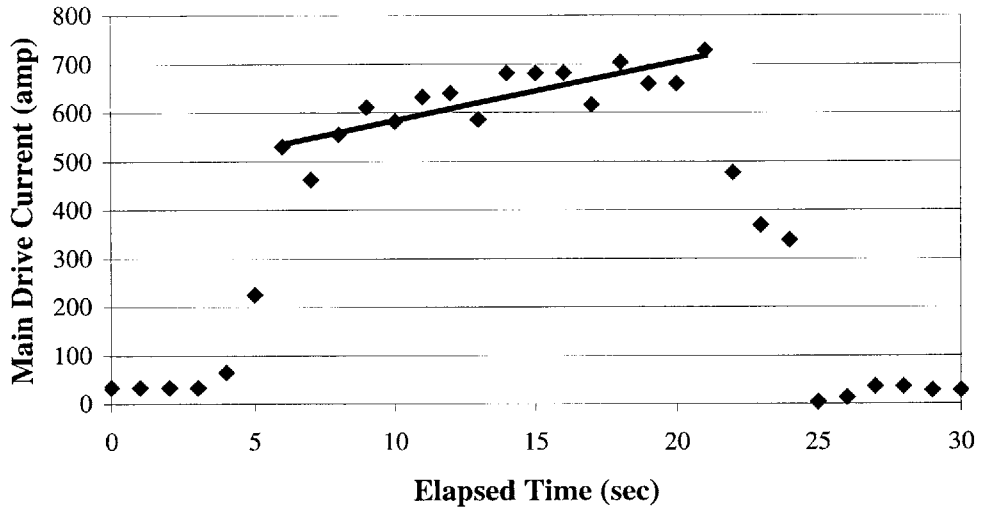

Figure F.1. *PRM main drive current for 13-add part at Research.*

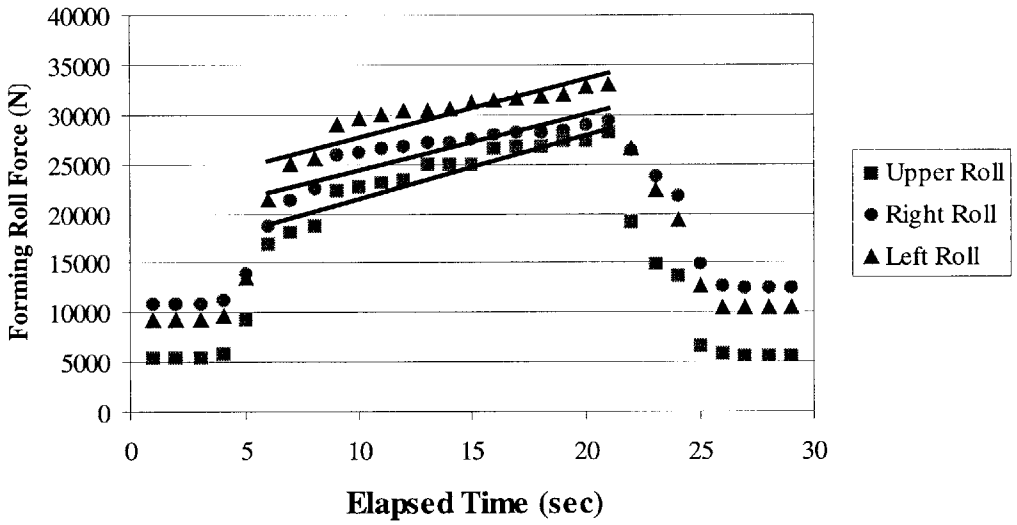

Figure F.2. *Forming roll forces for 13-add part at Research.*

Appendix G: Endnotes

Chapter 2

1. The DVG gauging system is proprietary property of The Timken Company.

Chapter 3

1. Profile Ring Team Technical Lecture Series, The Timken Company. October 1998.
2. Estimating the adiabatic heating effect was not simple at first because the amount of work done by the forming rolls was unknown. Also, the actual temperatures of the material and tooling inside the PRM were not known.
3. The complete equation is proprietary property of The Timken Company.
4. Tarnovskii, Pozdeyev, and Lyashkov. Deformation of Metals during Rolling. (Pergamon Press, 1965.)

   Pietrzyx and Lenard. Thermal-Mechanical Modelling of the Flat-Rolling Process. (Springer-Verlag, 1991.)

   Backofen, Walter. Deformation Processing. (Addison-Wesley, 1972.)
5. Kalpakjian. Serope. Manufacturing Engineering & Technology. 3rd Edition. (Addison-Wesley, 1995.)

Chapter 4

1. This does not include the first and last preforms, which are known to be non-uniform with the rest of the shell as discussed in Section 2.2. Preforms 23-28 were also removed from the trendline because they did not separate during forming.
2. Complete data is not available because of proprietary restrictions.